nature communications

Article

https://doi.org/10.1038/s41467-025-57631-x

Clade-specific extracellular vesicles from *Akkermansia muciniphila* mediate competitive colonization via direct inhibition and immune stimulation

Received: 31 August 2023

Accepted: 26 February 2025

Published online: 19 March 2025

Check for updates

Moon-Gi Hong[1,7], Eun-Ji Song[2,7], Hye Jin Yoon[3,7], Won-Hyong Chung[2], Hae Yeong Seo[3], Dohak Kim[1], Dokyung Lee[1], Jae-Gu Seo[1], Hayoung Lee[4,5], Seung Il Kim[4], Gwang Joong Kim[6], Kil-Nam Kim[6], Sang-Nam Lee[1] ✉, Kwang Soon Kim[3] ✉ & Young-Do Nam[2] ✉

Akkermansia muciniphila, a promising candidate for next-generation probiotics, exhibits significant genomic diversity, classified into several distinct clades (AmI to AmIV). Notably, a single *Akkermansia* clade tends to predominate within individual hosts, with co-occurrence of different clades being rare. The mechanisms driving such clade-specific exclusion remain unclear. Here, we show that extracellular vesicles (EVs) derived from AmII clade inhibit the growth of clade I (AmI), conferring a competitive advantage to AmII. Moreover, we observe clade-specific immunoglobulin A (IgA) responses, where AmII clade-specific IgAs, induced by EVs from AmII, facilitate niche occupancy and competitive exclusion of AmI. These findings provide insights into the competitive dynamics of *A. muciniphila* clades and suggest that future personalized microbiome interventions could be optimized by considering the clade composition of *A. muciniphila* in individual hosts.

Human microbiota, the trillions of microorganisms that inhabit the human body, have emerged as critical factors contributing to human health and disease[1,2]. Among the numerous species within gut microbiota, *Akkermansia muciniphila* has attracted considerable attention in recent years as a candidate for application in next-generation probiotics[3,4]. *A. muciniphila*, a mucin-degrading bacterium residing in the mucus layer of the gut, plays a pivotal role gut health maintenance and host homeostasis[5–8]. Reduced *A. muciniphila* levels have been linked to metabolic disorders such as obesity[8,9]. *A. muciniphila* ameliorates obesity-related symptoms by enhancing intestinal epithelial barrier functions[3,9,10] and promoting glucagon-like peptide-1 production in the intestinal epithelium[7]. Moreover, *A. muciniphila* has been identified as a key microbial species that can enhance anti-tumor immunotherapy efficacy based on immune checkpoint blockade treatment in both humans and mice[11,12]. However, experimental research has largely focused on the type strain (BAA-835) and a few newly isolated strains, limiting our understanding of the broader therapeutic potential of *A. muciniphila* strains.

Despite growing interest in *A. muciniphila*, the extent of its genetic diversity and the functional implications, in addition to its distribution across different populations, remain poorly understood. Previous pangenomic studies have identified four distinct clades of

[1]R&D Center, Enterobiome Inc., 814 Siksa-dong, Ilsandong-gu, Goyang-si, Republic of Korea. [2]Research Group of Personalized Diet, Korea Food Research Institute, 245 Nongsaengmyeong-ro, Iseo-myeon, Wanju-gun, Jeollabuk-do, Republic of Korea. [3]Department of Life Sciences, Pohang University of Science and Technology, Pohang, Republic of Korea. [4]Digital Omics Research Center, Korea Basic Science Institute, Cheongju, Republic of Korea. [5]Critical Diseases Diagnostics Convergence Research Center, Korea Research Institute of Bioscience and Biotechnology, Daejeon, Republic of Korea. [6]Gwangju Center, Korea Basic Science Institute (KBSI), Gwangju, Republic of Korea. [7]These authors contributed equally: Moon-Gi Hong, Eun-Ji Song, Hye Jin Yoon.
✉e-mail: snlee@enterobiome.com; kskim27@postech.ac.kr; youngdo98@kfri.re.kr

A. muciniphila (AmI to AmIV)[13–15]. AmII and AmIV clades have been proposed as novel species within the genus *Akkermansia*, based on phenotypic, phylogenetic, and genetic characteristics[16–18]. The subspecies-level genomic variability translates into phenotypic differences, particularly affecting host-microbe interactions[19,20]. Understanding *A. muciniphila* diversity within the host gut is therefore essential for uncovering its functional relevance to gut health and assessing its therapeutic potential across various diseases.

A. muciniphila colonization of the gut is a dynamic process, influenced by the host and environmental factors[21–23]. Previous studies have investigated the mechanisms underlying the colonization and persistence of *A. muciniphila* in the host gut, providing insights into its ecological role within the human gut[24,25]. Notably, within individual hosts, a single *A. muciniphila* clade typically predominates, with co-occurrence of multiple clades being relatively rare[15,26]. However, the global distribution pattern and population structure of such clade-typed *A. muciniphila* remain poorly understood. Furthermore, the mechanisms underlying the dominance of a single clade and co-exclusion between *A. muciniphila* clades are unclear. Single clade predominance of *A. muciniphila* clades in individual hosts further emphasizes the necessity of re-evaluating the correlation between *A. muciniphila* and beneficial health outcomes across different clades. Furthermore, stratifying the *A. muciniphila* types present in the host gut may facilitate the development of personalized therapeutic intervention.

Bacteria produce and release extracellular vesicles (EVs), including outer-membrane vesicles (OMVs), from Gram-negative bacteria[27,28]. The EVs mediate communication not only between bacteria but also with host cells[29]. Bacterial EVs regulate microbial interactions within microbial communities through various mechanisms. Bacterial EVs promote nutrient acquisition and deliver molecules with antimicrobial activities that target microbial competitors[29–31]. For instance, *Myxococcus xanthus* uses OMVs as cargo to deliver hydrolytic enzymes and antibiotics for killing prey microbes[31]. In addition, EVs produced by gut microbes or enteric pathogens can elicit immune responses[32] and modulate the functions of intestinal epithelial cells[33]. Furthermore, EVs produced by *A. muciniphila* can interact with intestinal epithelial cells, enhancing barrier function by regulating tight junctions[10,34]. However, despite the importance of EVs in microbial communication, the role of EVs produced by *A. muciniphila* in the single clade predominance remains largely unexplored.

Gut microbiota play a critical role in shaping intestinal adaptive immunity. Various gut microbes stimulate B cells to produce immunoglobulin A (IgA), which is secreted into the gut lumen. These anti-commensal IgAs serve diverse functions, such as toxin neutralization, prevention of pathogen infiltration, and promoting mucosal attachment of specific gut microbes. IgA facilitates the mucosal colonization of *Bacteroides fragilis* by enhancing intimate association with the gut mucosal surface[35–37]. *A. muciniphila* stimulates the adaptive immune system to produce *A. muciniphila*-specific antibodies[38]. However, it remains unclear whether this interaction between *A. muciniphila* and host immune system can influence the colonization dynamics of *A. muciniphila* and whether it plays a role in the single clade predominance.

Here, we explore the global distribution and population structure of clade-typed *A. muciniphila*, revealing that diversity of *A. muciniphila* in humans is influenced by urbanization and its clade predominance is widespread. Using in vitro co-culture experiments and gnotobiotic mice associated with both AmI and AmII in various conditions, we show that the co-exclusion of *A. muciniphila* clades is mediated through a combination of inter-clade inhibitory mechanisms and niche pre-occupation. Specifically, EVs derived from *A. muciniphila* clade II (AmII) unilaterally inhibit the growth of clade I (AmI), conferring a competitive advantage to AmII. Moreover, clade-specific immunoglobulin A (IgA) responses are observed. AmII clade-specific IgAs, induced by EVs from AmII, facilitate niche occupancy and competitive exclusion of AmI. These findings provide insights into the competitive dynamics of *A. muciniphila* clades and suggest that future personalized microbiome interventions could be optimized by considering the clade composition of *A. muciniphila* in individual hosts.

Results

A. muciniphila diversity influenced by urbanization and single clade predominance in human populations

We sequenced whole genomes of 44 newly isolated *A. muciniphila* strains and analyzed them together with 48 publicly-available genomes to investigate the genomic divergence of human-associated *A. muciniphila* genomes (Supplementary Data 1). Briefly, 16S rRNA phylogenetic analysis (Supplementary Fig. 1A) showed that the 92 *A. muciniphila* were classified into AmI ($n = 74$), AmII ($n = 13$), and AmIV ($n = 5$), as reported in previous studies[13–15]. Additionally, the *A. muciniphila* strains were equally classified according to average nucleotide identity analysis based on whole-genome comparison (Supplementary Fig. 1B). The functional classification and genomic diversity of the 92 *A. muciniphila* were also evaluated, which showed the inter-clade genetic distances (Supplementary results, Supplementary Table 1, Supplementary Data 2, 3, and Supplementary Fig. 2).

Although *A. muciniphila* can be classified into several clades (AmI–AmIV), studies on the global distribution of clade-typed *A. muciniphila* are scarce. Our previous study characterized the gut microbiome of 890 healthy Korean individuals using 16S rRNA sequencing, especially based on Amplicon Sequence Variant (ASV) analysis and microbial clusters[39]. ASV analysis was selected as it provides a higher resolution and allows precise identification of *A. muciniphila* clades[40]. We confirmed 22 ASVs belonging to *A. muciniphila* after taxonomic classification and aligned the ASVs with the 16S rRNA sequences of *A. muciniphila* genomes to identify their respective clades (Supplementary Fig. 3). The ASVs were classified into AmI ($n = 13$), AmII ($n = 8$), and AmIV ($n = 1$). Based on ASV analysis, we successfully examined the distribution of *A. muciniphila* clades in healthy Korean individuals. We identified the clades according to total read count ranking: among the ASVs classified into AmI, those that showed the highest total read count were named ASV_AmI_01. *A. muciniphila* was observed in 357 healthy Korean subjects (40.11%). A single *A. muciniphila* clade was dominant (mainly AmI or AmII) in healthy individual Korean hosts. In particular, the numbers of *A. muciniphila*-harboring Korean subjects with AmI, AmII, and AmIV were 237 (66.39%), 112 (31.37%), and 2 (0.56%), respectively (Fig. 1A), but the co-existence of two clades was observed in only 6 of the 357 subjects (1.68%) (Fig. 1B).

Based on ASV analysis, we also evaluated *A. muciniphila* clade distribution in the global human population (Fig. 1A and Supplementary Data 4). Overall, *A. muciniphila* had an incidence of 13.58–61.98% depending on the country; in 16 of the 22 countries, the predominant colonization of a single *A. muciniphila* clade was observed (mainly AmI or AmII). The co-existence of two clades was observed only in six countries: 1.32% in the USA, 2.20% in China, 5.81% in Sweden, 4.34 % in Canada, and 8.93% in Colombia (Fig. 1A, B). AmI and AmII were observed in all countries, excluding Republic of the Congo, where only AmI was identified. Notably, AmII and AmIV proportions tend to be high in countries with high urban rates (Fig. 1A, C).

To examine co-exclusion between *A. muciniphila* clades, Spearman correlation analysis was performed within (intra-clade) and between clades (inter-clade) for *A. muciniphila* clades according to ASV analysis in Korean subjects (Fig. 1D). An overall positive correlation within clades was observed, except for one case (AmI_01 vs AmI_02, coefficient strength: −0.27, p-value < 2.387e-07). However, a negative correlation was observed between clades (AmI vs AmII). This was especially true for AmI_01 and AmII_01 ASV, which had the highest read count and a strong negative correlation (coefficient strength: −0.66, p-value < 2.2e-16). In other countries, top-ranked AmI strains

https://doi.org/10.1038/s41467-025-57631-x

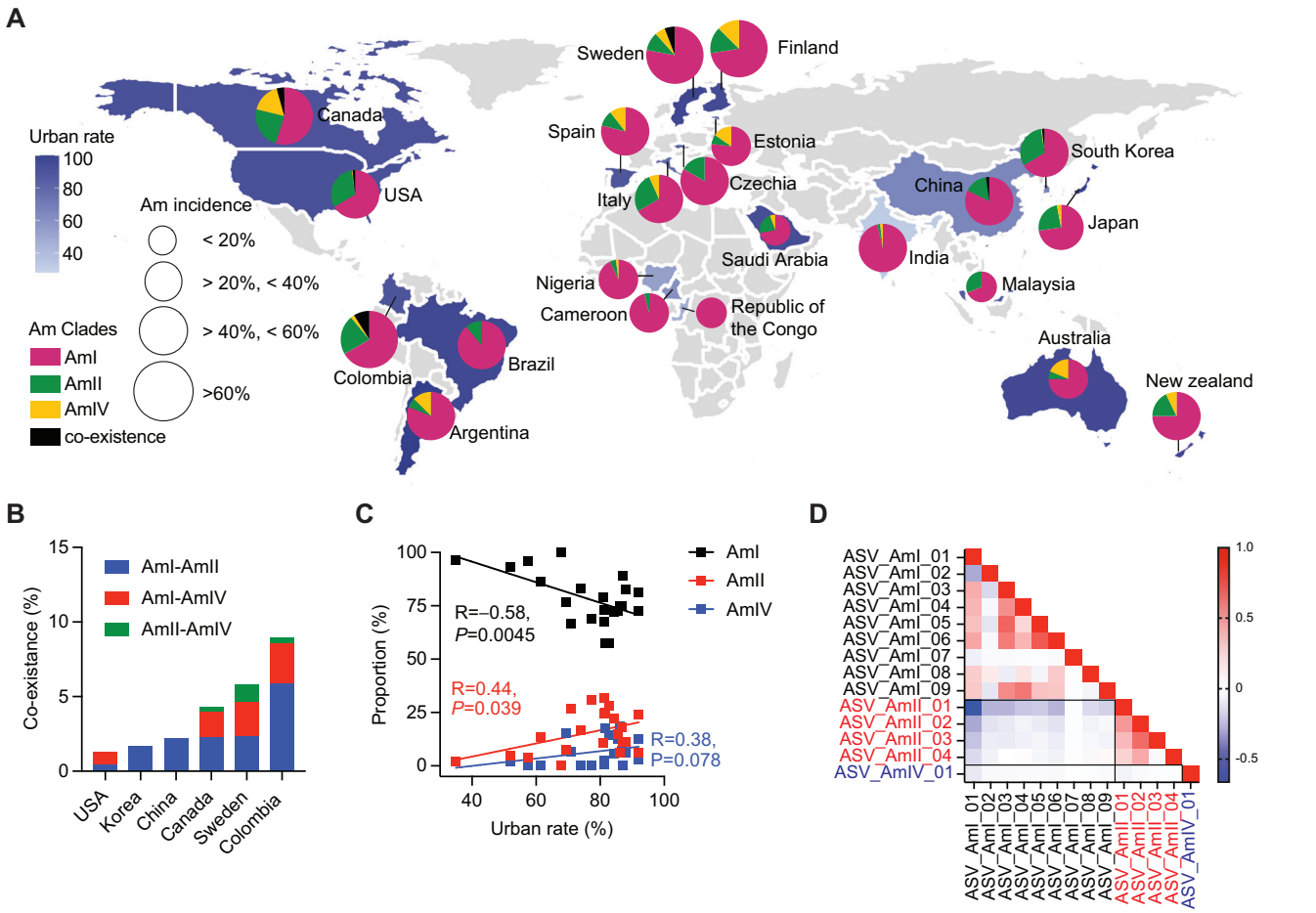

Fig. 1 | Diversity of *A. muciniphila* influenced by urbanization and single clade predominance in human populations. A Pie charts showing the distribution of *A. muciniphila* clades within each country. The blue scale filling each country represents the urban rate. The size of the pie reflects the proportions of individuals harboring *A. muciniphila* in each country. **B** Coexistence of *A. muciniphila* clades in six countries. **C** Scatter plot with Pearson correlation coefficients after two-sided multiple comparisons showing the correlation between the proportion of *A. muciniphila* clades and urbanization rate. **D** Spearman correlation matrix of *A. muciniphila* ASVs according to clade in 890 healthy Korean subjects. Spearman correlation coefficient strength was 12 as indicated by the colored bar. Twenty-two *A. muciniphila* ASVs were named for each clade according to the rank of total read count, and 14 ASVs with >1000 read count were used for correlation analysis (ASV_AmI_01 to ASV_AmI_09: black, ASV_AmII_01 to ASV_AmII_04: red, ASV_AmIV_01: blue). Source data are provided as a Source Data file.

were similarly positively correlated with the other AmI strains but negatively correlated with AmII strains (Supplementary Fig. 4).

The co-existence of multiple *A. muciniphila* strains within the same clade could be identified by the presence of multiple ASVs in an individual. The proportion of individuals harboring multiple ASVs varied across different countries (Supplementary Fig. 5). In regions where co-existence of strains from different clades was low or not observed, individuals with multiple ASVs from the same clade was more frequently observed. For instance, in the Korean populations, the proportions of individuals with multiple ASVs in the AmI and AmII clade were 34.5% and 24.1%, respectively, suggesting that *A. muciniphila* strains within the same clade can co-exist, while being mutually exclusive with strains from other clades (Supplementary Fig. 5). Overall, the findings suggest that *A. muciniphila* clade diversity in human populations is influenced by urbanization, and single clade predominance of *A. muciniphila* is a widespread feature, regardless of ethnicity and global location.

Culture supernatants from various AmII clade strains unilaterally inhibit AmI clade growth in vitro

Given the observed predominance of either AmI or AmII clades in the human gut microbiome, we aimed to investigate the mechanisms underlying co-exclusion between the clades. Previous reports have shown that AmI clades possess a higher genetic capacity for adapting to the human intestinal environment, particularly through their ability to utilize mucin-related substrates, and they exhibit faster doubling times compared to AmII clades[15]. Consequently, it has been assumed that AmI could outcompete AmII owing to its superior ability to exploit nutritional resources in the host gut. AmI strains possess specific genes involved in assimilatory sulfate reduction (ASR), which aids in mucin utilization (Supplementary Fig. 6 and Supplementary Data 2, 3). Some essential ASR genes were absent in AmII strains. Although we did not observe difference in growth rates between the representative AmI and AmII strains, EB-AMDK19 and EB-AMDK39, respectively, in vitro, presumably due to the nutrient-enriched media, the depletion of L-cysteine inhibited the growth of EB-AMDK39 in vitro significantly (Supplementary Fig. 6), further indicating potential metabolic vulnerability of AmII strains.

To examine competition between the *A. muciniphila* clades, an in vitro co-culture experiment was performed using EB-AMDK19 (AmI) and EB-AMDK39 (AmII) strains. Each *A. muciniphila* clade was detected and quantified by qPCR with clade-specific primers. Unexpectedly, EB-AMDK39 outcompeted EB-AMDK19, becoming obviously predominant subsequently, after 24 h of co-inoculation (Fig. 2A). These results suggest that AmII possesses competitive advantages over AmI despite lacking essential ASR genes.

https://doi.org/10.1038/s41467-025-57631-x

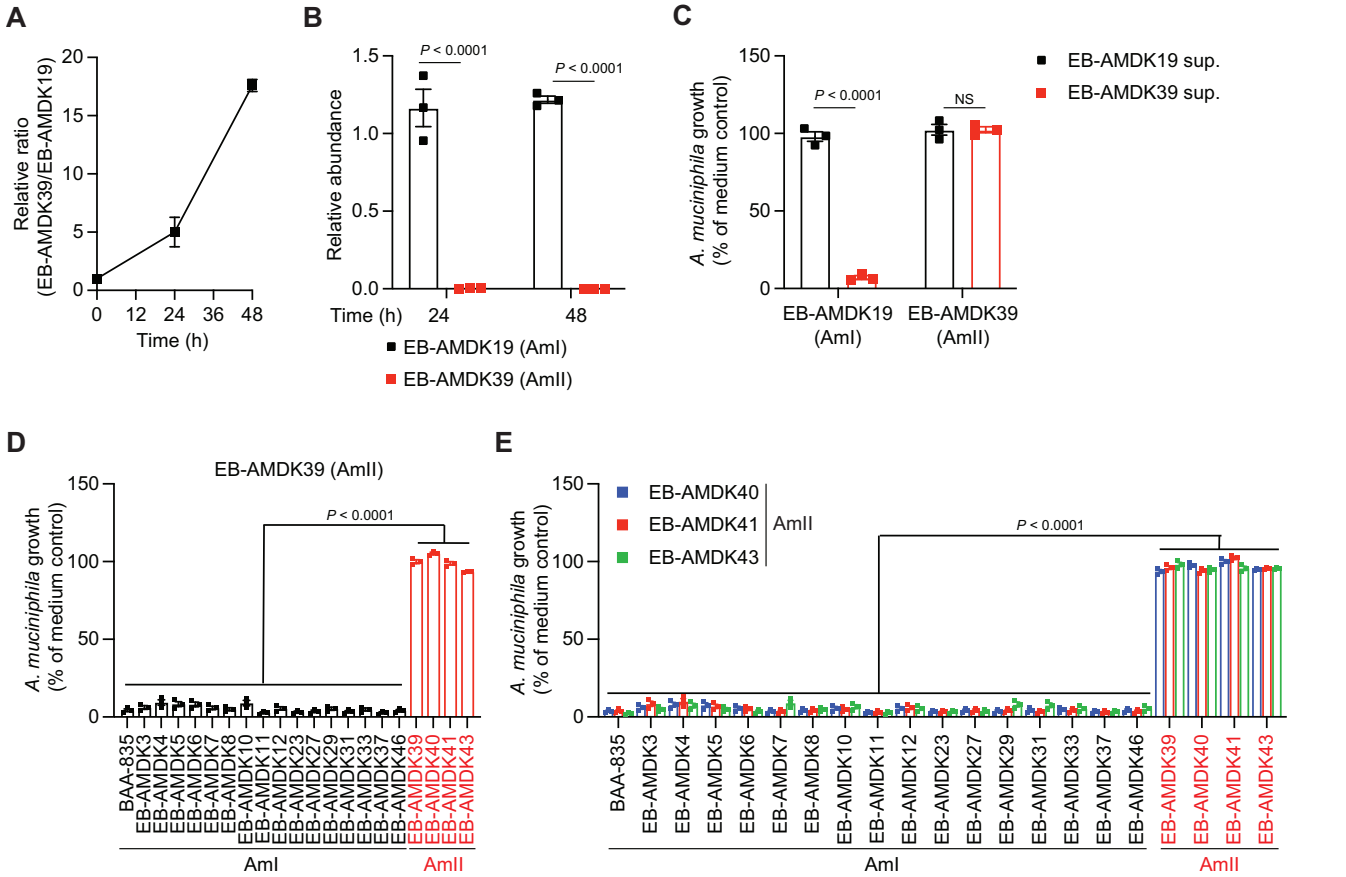

Fig. 2 | Culture supernatants from various AmII clade strains unilaterally inhibit AmI clade growth in vitro. A Changes in relative abundance of EB-AMDK19(AmI) and EB-AMDK39 (AmII) after in vitro co-culture. Equal numbers of EB-AMDK19 and EB-AMDK39 were co-inoculated into mucin-rich media. Values are averaged from three biological replicates. **B** Changes in relative abundance of *A. muciniphila* clades upon addition of EB-AMDK39 to EB-AMDK19-enriched culture. EB-AMDK39 (1×10^8 CFU) was additionally inoculated into EB-AMDK19-enriched culture (1×10^{10} CFU/culture). **C** Changes in growth of EB-AMDK19 (AmI) and EB-AMDK39 upon the treatment with culture supernatants derived from EB-AMDK19 and EB-AMDK39. **D**, **E** Changes in growth of various *A. muciniphila* strains belonging to AmI and AmII clades upon treatment with supernatants derived from the EB-AMDK39 (**D**) and from the other AmII clade strains (**E**). Growth of each *A. muciniphila* strain was measured as OD_{600} at 48 h after inoculation (AmI strains: black, AmII strains: red). Growth was depicted as a percentage of media control ($n = 3$ biological replicates). Cell-free supernatants derived from *A. muciniphila* strains were prepared through filtration (0.2 μm). At least, two independent experiments showed similar results. Statistical differences were determined using two-way ANOVA with Sidak's multiple comparison tests. ns: not significant. Error bars represent SEM. Source data are provided as a Source Data file.

Next, we examined whether pre-occupancy of a specific *A. muciniphila* clade could prevent colonization of another clade introduced subsequently. EB-AMDK39 was inoculated at a concentration of 1×10^8 CFU into an EB-AMDK19-enriched culture (1×10^{10} CFU/culture). Under the conditions, EB-AMDK19 remained predominant and EB-AMDK39 was barely detectable (Fig. 2B), suggesting that the niche pre-occupied by AmI could prevent subsequent AmII colonization.

To investigate the mechanisms behind the competitive advantage of AmII over AmI, we examined whether the culture supernatants of AmII have inhibitory effects on AmI growth. Notably, EB-AMDK39-derived supernatants inhibited the growth of EB-AMDK19 severely but had no effect on EB-AMDK39 itself (Fig. 2C). In contrast, supernatants derived from EB-AMDK19 did not impact the growth of either EB-AMDK19 or EB-AMDK39, indicating that the inhibitory effects are specific to AmII-derived supernatants (Fig. 2C).

Next, to examine whether the inhibitory effect of AmII-derived supernatant was consistent across various strains, the cultures with various AmI strains were treated with EB-AMDK39-derived supernatants, including BAA-835, as well as AmII strains (EB-AMDK39, −40, −41, and −43). As expected, EB-AMDK39-derived supernatants inhibited the growth of all tested AmI strains but did not affect the growth of AmII strains (Fig. 2D). Conversely, supernatants derived from AmII strains other than EB-AMDK39 also inhibited the growth of various AmI strains but not AmII strains (Fig. 2E).

Culture supernatants derived from both AmI and AmII strains contain mucin from porcine stomach. To exclude the possibility that the biotic components in the porcine mucus in AmII-derived supernatants mediate AmI growth inhibition, the inhibitory effect of EB-AMDK39-derived supernatants from the culture under mucin-free conditions on EB-AMDK19 growth were tested. Mucin-free EB-AMDK39-derived supernatants also effectively inhibited the growth of EB-AMDK19 but not EB-AMDK39, suggesting that biotic contaminant derived from porcine mucus does not mediate AmI growth inhibition (Supplementary Fig. 7). Overall, these findings suggest that the specific components in AmII-derived supernatants are key players in the competitive exclusion of AmI clades in co-culture conditions.

Extracellular vesicles derived from AmII inhibit AmI growth in vitro

Next, we sought to determine the characteristics of components in AmII-derived supernatants, which mediate AmI growth inhibition, through various conditions (Fig. 3). The inhibitory effect of EB-AMDK39 (AmII)-derived supernatant on EB-AMDK19 (AmI) growth was abolished by heat inactivation but not by proteinase K

https://doi.org/10.1038/s41467-025-57631-x

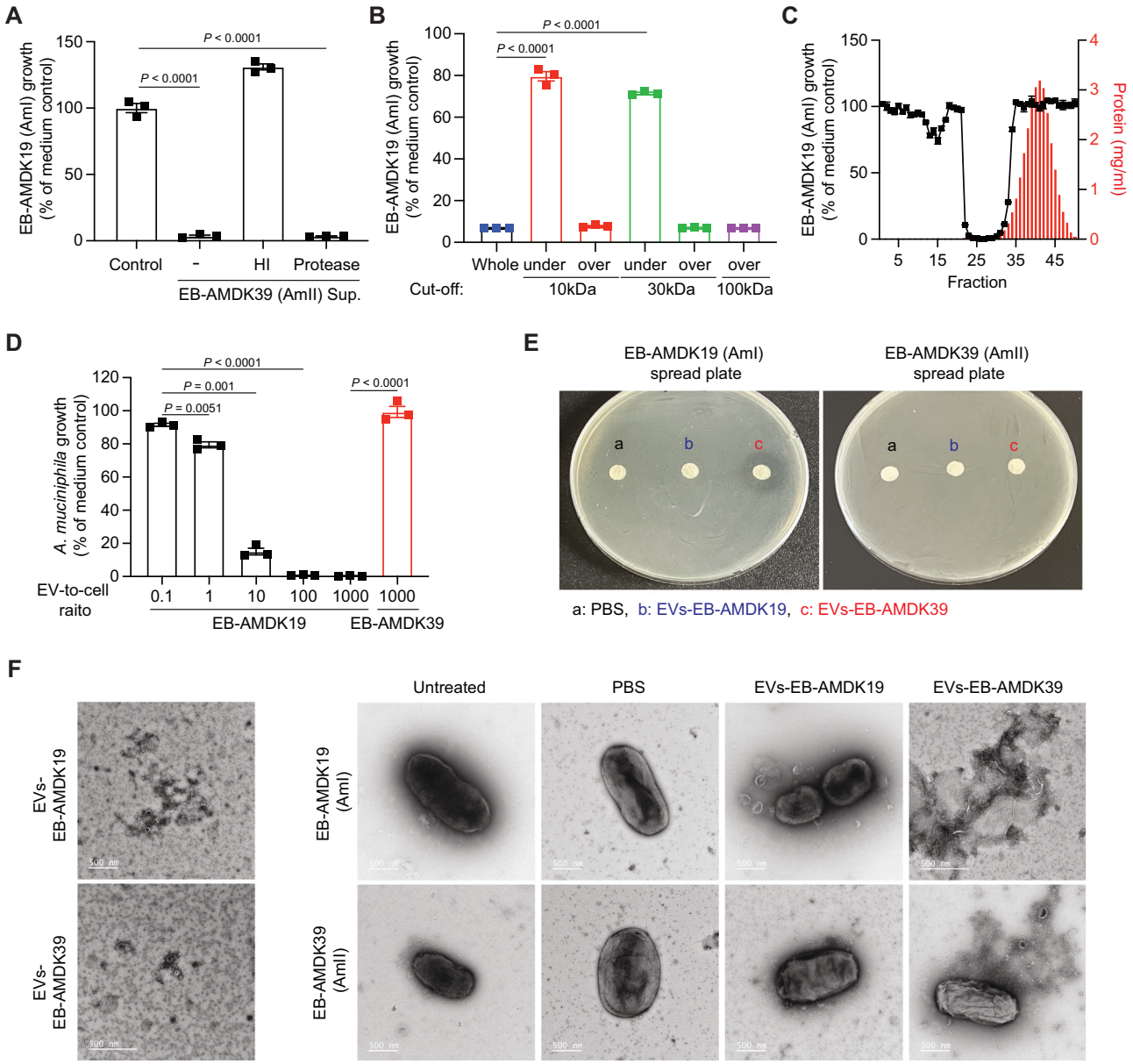

Fig. 3 | Extracellular vesicles derived from AmII inhibit AmI growth in vitro. **A** Changes in EB-AMDK19 (AmI) growth upon treatment with unprocessed, heat-inactivated (HI) and protease-treated EB-AMDK39 (AmII)-derived culture supernatant. AmII-derived supernatants were heat-inactivated at 95 °C for 15 min or treated with proteinase K (1 mg/mL) for 16 h at 37 °C. Proteinase K-treated samples were supplemented with protease inhibitor (1 mM). **B** EB-AMDK19 growth inhibition by EB-AMDK39-derived culture supernatant fractionated by molecular weight. EB-AMDK19 growth was assessed after 24 h in the presence of 20% size-fractionated EB-AMDK39-derived culture supernatant. **C** Identification of inhibitory size-exclusion fractions derived from EB-AMDK39-derived culture supernatant. Fractions prepared by size-exclusion chromatography were treated into EB-AMDK19 culture at a final concentration of 10% (v/v). Growth of EB-AMDK19 at 37 °C for 24 h was depicted as a percentage of media control. Points and connecting lines are drawn to show the EB-AMDK19 growth changes according to the fractions. Column bar graph shows the protein concentration (mg/mL) in each fraction. **D** Dose dependent inhibition of EB-AMDK19 growth by enriched EB-AMDK39-derived EVs. EV particle number was determined by nano particle tracking analysis. Enriched EB-AMDK39-derived EVs at various EV-to-cell ratios were used to treat EB-AMDK19 culture (1×10^6 CFU/culture) and growth was assessed after 24 h. **A**–**D** Growth is depicted as a percentage of media control ($n = 3$ biological replicates). At least, two independent experiments showed similar results. Statistical differences were determined by one-way ANOVA with Tukey's multiple comparison tests. ns: not significant. Error bars represent SEM. **E** Disk diffusion test to monitor the growth inhibition of each clades by enriched EVs derived from EB-AMDK19 (EVs-EB-AMDK19) and EB-AMDK39 (EVs-EB-AMDK39). **F** Transmission electron micrographs showing enriched EVs derived from EB-AMDK19 or EB-AMDK19 and the structural integrity of each clade strain upon treatment with enriched EVs derived from EB-AMDK19 or EB-AMDK19. Bars indicate 500 nm. At least two independent experiments showed similar results. Source data are provided as a Source Data file.

treatment, indicating that the inhibitory components are thermolabile yet resistant to proteinase digestion (Fig. 3A). Furthermore, fractions of EB-AMDK39 -derived supernatants with molecular weights < 30 kDa lost their inhibitory effect on EB-AMDK19 growth, while fractions > 100 kDa remained effective in inhibiting the EB-AMDK19 growth (Fig. 3B).

To identify the specific inhibitory component, size-exclusion chromatography was performed using Sepharose CL-6B and fractionated EB-AMDK39-derived supernatants. The inhibitory effect of each fraction on EB-AMDK19 growth was tested. The inhibitory activity was observed in fractions (fractions 22–33) eluted before free proteins, typically containing EVs (Fig. 3C)[41–44]. EVs were clearly detected

($1.19 \pm 0.08 \times 10^9$ particles/mL and 237.53 ± 22.34 nm) in the fractions (mostly 25–29 fractions) through nanoparticle tracking analysis. Transmission Electron Microscopy (TEM) further confirmed the presence and morphology of EVs in the fractions (Supplementary Fig. 8). Notably, treatment with AmII-derived fractions containing EVs led to morphological changes in AmI, including loss of structural integrity (Supplementary Fig. 8).

We further enriched EVs from the EB-AMDK39 (AmII) clade via ultra-centrifugation ($1.67 \pm 0.13 \times 10^{12}$ particles/mL and particles size of 214.77 ± 0.74 nm) and used them to treat EB-AMDK19 (AmI) at EV-to-cell ratios ranging from 0.1 to 1000 and EB-AMDK39 at EV-to-cell ratios of 1000 (Fig. 3D). Notably, EVs were enriched from mucin-free cultures. Enriched EB-AMDK39-derived EVs effectively suppressed EB-AMDK19 growth in a dose-dependent manner, with no effect on the growth of EB-AMDK39 (Fig. 3D). Complete inhibition of EB-AMDK19 growth was observed when the ratio of EB-AMDK39-derived EV particles to EB-AMDK19 cells was 100-fold or higher. No inhibition was observed when the EV-to-cell ratio was less than 1:1. This threshold response of enriched EB-AMDK39-derived EVs likely contributes to the pre-occupancy effect driving competitive exclusion between AmI and AmII. Considering that 1 mL of EB-AMDK39-derived culture supernatant from the stationary phase was treated to an EB-AMDK19 culture with 10^6 bacteria (Fig. 2C), the EVs were estimated to be present at a concentration of $\geq 10^8$ particles/mL in the EB-AMDK39-derived culture supernatant. EVs produced by EB-AMDK39 during both mid-log and stationary growth phase consistently inhibit the growth of EB-AMDK19 when EV-to-cell ratio was 100-fold higher, indicating that EB-AMDK39 produces EVs with inhibitory activity regardless of growth phase (Supplementary Fig. 9A–C). A disk diffusion assay also confirmed the findings. A clear zone was only observed near a disk containing enriched EB-AMDK39-derived EVs on an EB-AMDK19-spread agar plate (Fig. 3E). Additionally, treatment with enriched EB-AMDK39-derived EVs induced structural changes in EB-AMDK19 cells but not in EB-AMDK39 cells (Fig. 3F).

To identify potential inhibitory components in enriched AmII-derived EVs, proteomic analyses were conducted to compare the protein profiles between whole cell lysates and EVs-enriched supernatant fractions, both derived from EB-AMDK39 and EB-AMDK19 (Supplementary Data 5). The analyses revealed that six distinct rearrangement hotspot (Rhs) repeat proteins were more abundant in the enriched EVs derived from EB-AMDK39, but not in those from EB-AMDK19, when compared with whole cell lysates (Supplementary Fig. 10A, B). Rhs repeat proteins are expressed and exported through the type VI secretion system in Gram-negative bacteria[45]. Rhs repeat proteins mediate inter-bacterial competition via their C-terminal toxin (CT) domain, which inhibits the growth of target bacteria[46,47]. However, Rhs-CT domain can be neutralized by cognate immunity Rhs proteins (RhsI) produced by the same bacteria[46,47]. These C-terminal toxin domains exhibit various enzyme activities, such as DNase, RNase, deaminase, peptidase, and pore-forming activities[47]. Therefore, the growth inhibition and loss of structural integrity in EB-AMDK19 upon treatment with EB-AMDK39-derived EVs might be attributed to the activity of Rhs repeat proteins. Furthermore, genomic analyses revealed that the genes encoding these Rhs repeat proteins are absent in AmI strains (Supplementary Fig. 10C). Rhs repeat proteins can be classified into 10 distinct groups and the genes encoding Rhs repeat proteins that were highly abundant in EB-AMDK39-derived EVs were only present in the AmII genome (Supplementary Fig. 10D, E). Collectively, the results suggest that AmII-derived EVs serve as a key inhibitory factor for AmI growth.

Luminal EVs derived from AmII-associated germ-free mice inhibit AmI growth in vitro

Next, we investigated whether AmII strains in the gut of germ-free (GF) mice produce EVs and whether the luminal EVs can inhibit AmI growth in vitro. We first mono-colonized GF mice with EB-AMDK19 (AmI) and EB-AMDK39 (AmII) strains (Fig. 4A, B). Both strains colonized the murine gut of GF mice successfully. EB-AMDK19 exhibited a faster colonization rate in the gut lumen than EB-AMDK39, presumably due to AmI's superior capacity for mucin utilization (Fig. 4A, B).

Treatment of whole fecal soluble fraction (SF) from GF mice did not affect the growth of both *A. muciniphila* strains (Fig. 4C, D). However, whole fecal SF from EB-AMDK39-associated GF mice effectively inhibited EB-AMDK19 growth but not EB-AMDK39 growth (Fig. 4C, D). As expected, heat-inactivated SF or fecal SF below 30 kDa from EB-AMDK39-associated GF mice did not affect EB-AMDK19 growth, whereas fecal SF > 100 kDa effectively inhibited EB-AMDK19 growth (Fig. 4C).

To compare the growth inhibitory effect of EVs derived from in vitro-cultured AmII, we performed size-exclusion chromatography on fecal SF from GF and EB-AMDK39-associated GF mice and assessed the inhibitory effects of each fraction on AmI growth. As expected, fractions from GF mice did not inhibit the growth of either *A. muciniphila* clade (Fig. 4E). However, fractions (20–27) derived from the fecal SF of EB-AMDK39-associated GF mice, which eluted before free proteins, inhibited EB-AMDK19 growth, without affecting EB-AMDK39 growth (Fig. 4E). Using the disk diffusion test, we also confirmed that minimally processed fecal SF from EB-AMDK39-associated GF mice could inhibit EB-AMDK19 growth (Fig. 4F). The results suggest that AmII strain in the host gut produces EVs that inhibit AmI growth, contributing to the observed predominance of single *A. muciniphila* clades in the human gut.

AmII strains of *A. muciniphila* predominate in the host gut under various conditions

To examine the colonization dynamics between AmI and AmII clades in vivo, gnotobiotic mice colonized with either EB-AMDK19 (AmI) or EB-AMDK39 (AmII) were generated. To explore the pre-occupancy effect on the competitive exclusion between the clades, GF mice were sequentially colonized with EB-AMDK19 followed by EB-AMDK39, or vice versa (Fig. 5A, B). The pre-occupied *A. muciniphila* clade (AmI or AmII) in the host gut could not be displaced by the subsequent administration of the other clade (Fig. 5A, B). Specifically, the initial colonization levels of pre-occupied clade reached 1×10^{10} genome equivalents/g feces and this level was not affected significantly by the introduction of the opposite clade.

Next, competition between AmI and AmII clades to occupy the vacant niche in the gut was investigated by co-administering both clades into GF mice (Fig. 5C). Initially, EB-AMDK19 dominated the gut, accounting for over 99% of the population (~ 10^{10} genome equivalents/g feces). However, within 4 days post co-administration, EB-AMDK19 decreased rapidly while EB-AMDK39 increased significantly (Fig. 5C). Consistent with the in vitro co-culture test of AmI and AmII strains, EB-AMDK39 outcompeted EB-AMDK19 in the host gut. The results suggest that the pre-occupancy and unilateral inhibitory effects of AmII on AmI growth can influence the predominance of specific *A. muciniphila* clades in the host gut.

To further examine the interactions between various *A. muciniphila* strains, GF mice were colonized with a mixture of three AmI strains (BAA-835, EB-AMDK7 and EB-AMDK23), both with and without AmII strains (either EB-AMDK39 or EB-AMDK43). Each *A. muciniphila* strain was detected and quantified by qPCR with strain-specific primers. In GF mice associated with the three AmI strains alone, although their levels were not equivalent, all strains were persistently above the detection limit, suggesting that AmI strains can co-exist in the gut, similar to observations in humans (Fig. 5D). However, in GF mice co-colonized with the three AmI strains and AmII strains (EB-AMDK39 or EB-AMDK43), the AmI strains were detectable only at the early time point (day 4 post co-administration) but dropped below the detection limit at later time points, indicating that AmII clade strains generally outcompete AmI clade strains in the gut (Fig. 5E, F).

https://doi.org/10.1038/s41467-025-57631-x

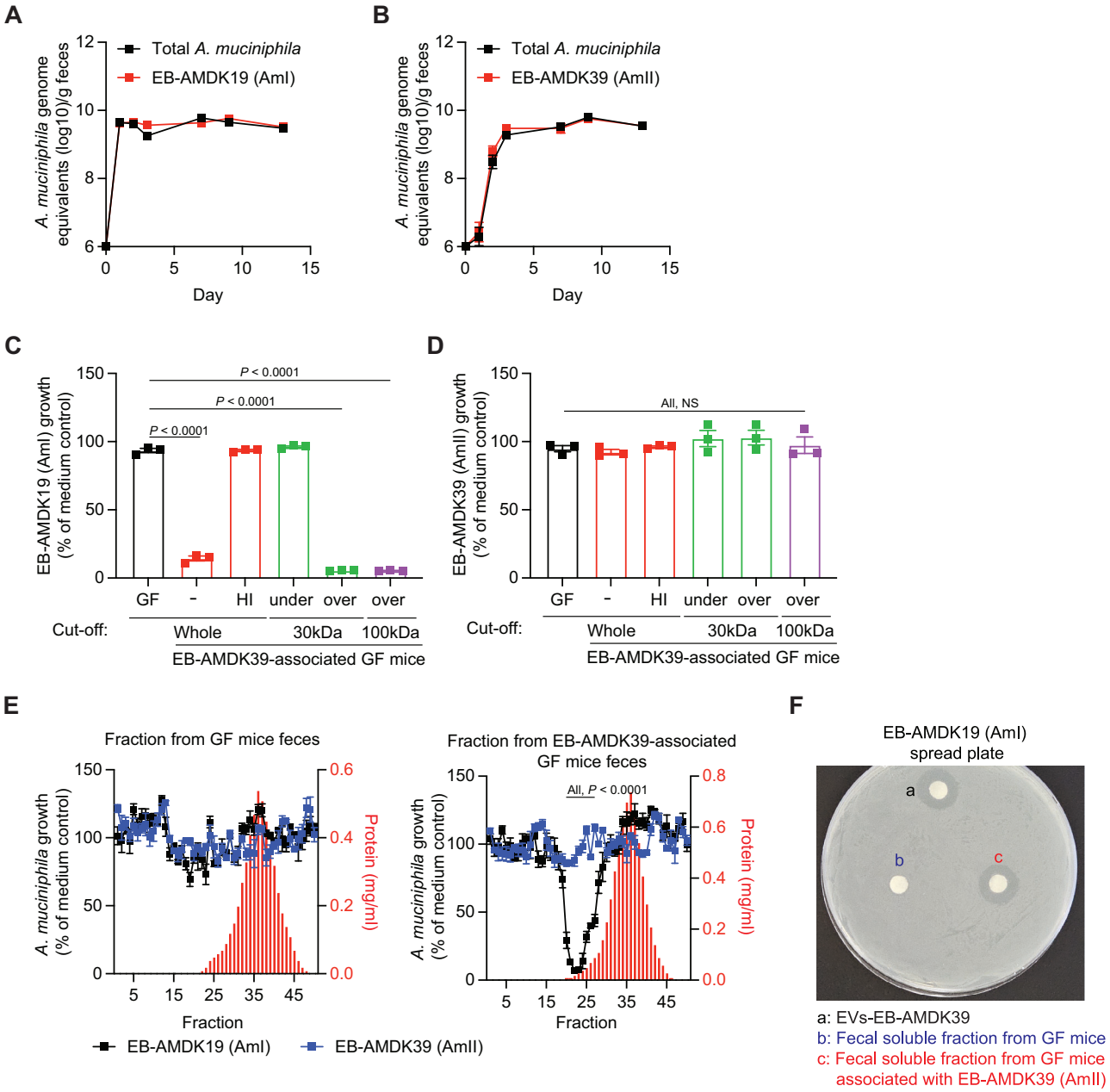

Fig. 4 | Luminal EVs derived from AmII-associated germ-free mice inhibit AmI growth in vitro. A, **B** Levels of EB-AMDK19 (AmI) (**A**) and EB-AMDK39 (AmII) (**B**) in feces from mono-associated GF mice at different time points. GF mice were gavaged with each clade and fecal DNA was prepared to determine luminal levels of each clade by qPCR ($n = 4$). **C**, **D** Changes in growth of EB-AMDK19 (**C**) and EB-AMDK39 (**D**) in vitro upon treatment of whole fecal soluble fractions (SF) from GF mice, and whole fecal SF, heat-inactivated whole fecal SF, and size-fractionated SF with indicated cut-off from EB-AMDK39-associated GF mice. Growth was assessed after 24 h upon treatment. Growth is depicted as a percentage of media control ($n = 3$ biological replicates). At least two independent experiments showed similar results. Statistical differences were determined by one-way ANOVA with Tukey's multiple comparison tests. ns: not significant. Error bars represent SEM. **E** Identification of inhibitory size-exclusion fractions derived from fecal SF of GF (left) and EB-AMDK39-associated GF mice (right). Fractions prepared by size-exclusion chromatography were used to treat EB-AMDK19 and EB-AMDK39 culture at a final concentration of 20% (v/v). Growth of each clade at 37 °C for 24 h is depicted as a percentage of media control. Points and connecting lines were drawn based on the clade growth patterns (% of medium control) according to the fractions. Growth of EB-AMDK19 and EB-AMDK39 was marked in black and blue, respectively. The column bar graph was drawn using the protein concentration (mg/mL) in each fraction (red). Data represent the averages of triplicate measurements. Two independent experiments showed similar results. Statistical differences were determined by two-way ANOVA with Sidak's multiple comparison tests. Error bars represent SEM. **F** Disk diffusion test to show changes in growth of EB-AMDK19 upon treatment with enriched EVs from EB-AMDK39 in vitro culture, fecal SF derived from GF (**B**), and EB-AMDK39-asssociated GF mice (**C**). Source data are provided as a Source Data file.

Additionally, we investigated the co-exclusion between different *A. muciniphila* clades in the presence of other commensal bacteria, such as Altered Schaedler Flora (ASF), a consortium of eight anaerobic bacteria. A mixture of EB-AMDK19 and EB-AMDK39 was administered into ASF-associated GF mice (Fig. 5G). The presence of ASF reduced the luminal levels of *A. muciniphila* significantly (Fig. 5H). The overall level of *A. muciniphila* in the presence of ASF was approximately 100-fold lower than those in *A. muciniphila* mono-associated GF mice (Fig. 5I). Nevertheless, *A. muciniphila* was able to stably colonize the gut with EB-AMDK39 remaining predominant (Fig. 5I). Overall, the results

https://doi.org/10.1038/s41467-025-57631-x

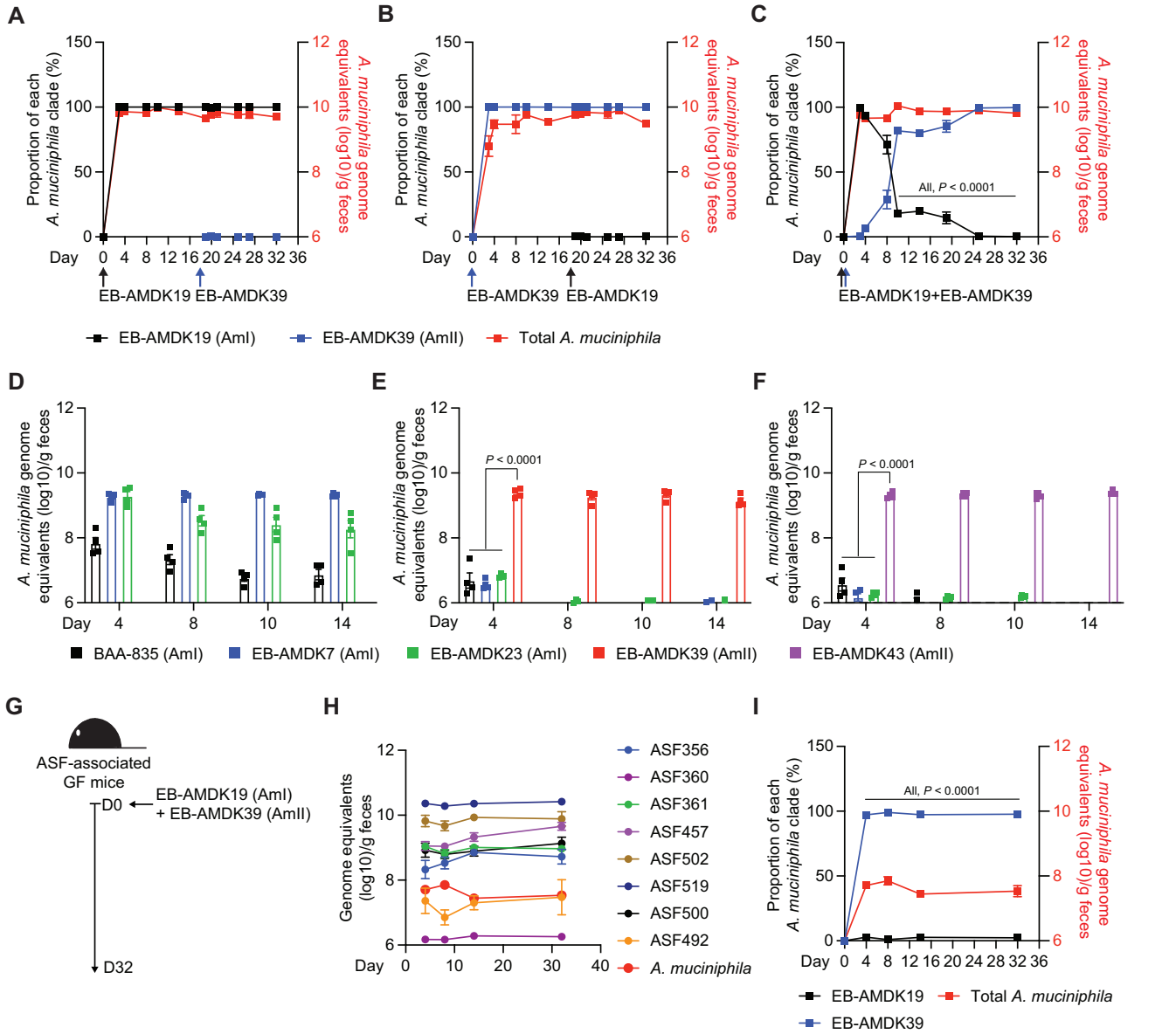

Fig. 5 | AmII strains of *A. muciniphila* predominate in the host gut under various conditions. A, **B** Pre-occupancy effect on competitive exclusion between AmI and AmII. **A** GF mice were first gavaged with EB-AMDK19 (AmI) followed by association with EB-AMDK39 (AmII) on day 19 post-EB-AMDK19 administration ($n = 4$). **B** GF mice were first gavaged with EB-AMDK39 followed by association with EB-AMDK19 on day 19 post-EB-AMDK39 administration ($n = 4$). **C** Competitive exclusion between AmI and AmII in the murine gut. GF mice were administered simultaneously with an equal mixture of two-clade strains ($n = 4$). The genome equivalent levels of total *A. muciniphila* and each clade in feces was quantified using qPCR with *A. muciniphila*-specific and clade-specific primers. The proportion of each clade (%) is shown as black points/line (EB-AMDK19) and blue points/line (EB-AMDK39). Each point represents the average of measurement in an individual mouse. Two independent experiments showed similar results. **D**–**F** GF mice were gavaged with a mixture of three AmI strains (BAA-835, EB-AMDK7, EB-AMDK23) alone (**D**) and with either EB-AMDK39 (AmII) (**E**) or EB-AMDK43 (AmII) (**F**) ($n = 4$). The genome equivalent levels of each *A. muciniphila* strain in feces was quantified using qPCR with strain-specific primers. Each point represents the average measurement in an individual mouse. **G**–**I** Competitive exclusion between *A. muciniphila* clades in gnotobiotic mice associated with Altered Schaedler Flora (ASF). **G**–**I** GF mice were first gavaged with ASF for 6 weeks. ASF-associated GF mice were administered with an equal mixture of two-clade strains (EB-AMDK19 and EB-AMDK39) ($n = 3$). **G** Experiment scheme. **H** Changes in the genome equivalent levels of ASF species and *A. muciniphila* ($n = 3$). **I** Competitive exclusion between EB-AMDK19 and EB-AMDK39 in the gnotobiotic mice ($n = 3$). The genome equivalent levels of total *A. muciniphila* and each clade in feces was quantified using qPCR with *A. muciniphila*-specific and clade-specific primers. The proportion of each clade (%) is shown as black points/line (EB-AMDK19) and blue points/line (EB-AMDK39). Each data point represents the average of measurements taken from an individual mouse. Two independent experiments showed similar results. Statistical differences were determined using two-way ANOVA with Sidak's multiple comparison tests (**A**–**I**). Error bars represent SEM. Source data are provided as a Source Data file.

suggest that AmII outcompetes AmI in the host gut under various conditions.

EV-induced clade-specific IgA enhances initial colonization of AmII in the host gut

Various commensal bacteria can induce cognate adaptive immune responses during homeostasis[48–50]. *A. muciniphila* also triggers adaptive immune responses, including both specific IgA as well as IgG responses[38]. Anti-commensal IgA can enhance the aggregation and colonization of a particular bacteria by facilitating bacterial adhesion to mucosal layers[35]. Therefore, it is plausible that *A. muciniphila* induces the production of luminal IgA to facilitate its colonization in the host gut. We investigated the effect of mono-association with different *A. muciniphila* clades on adaptive

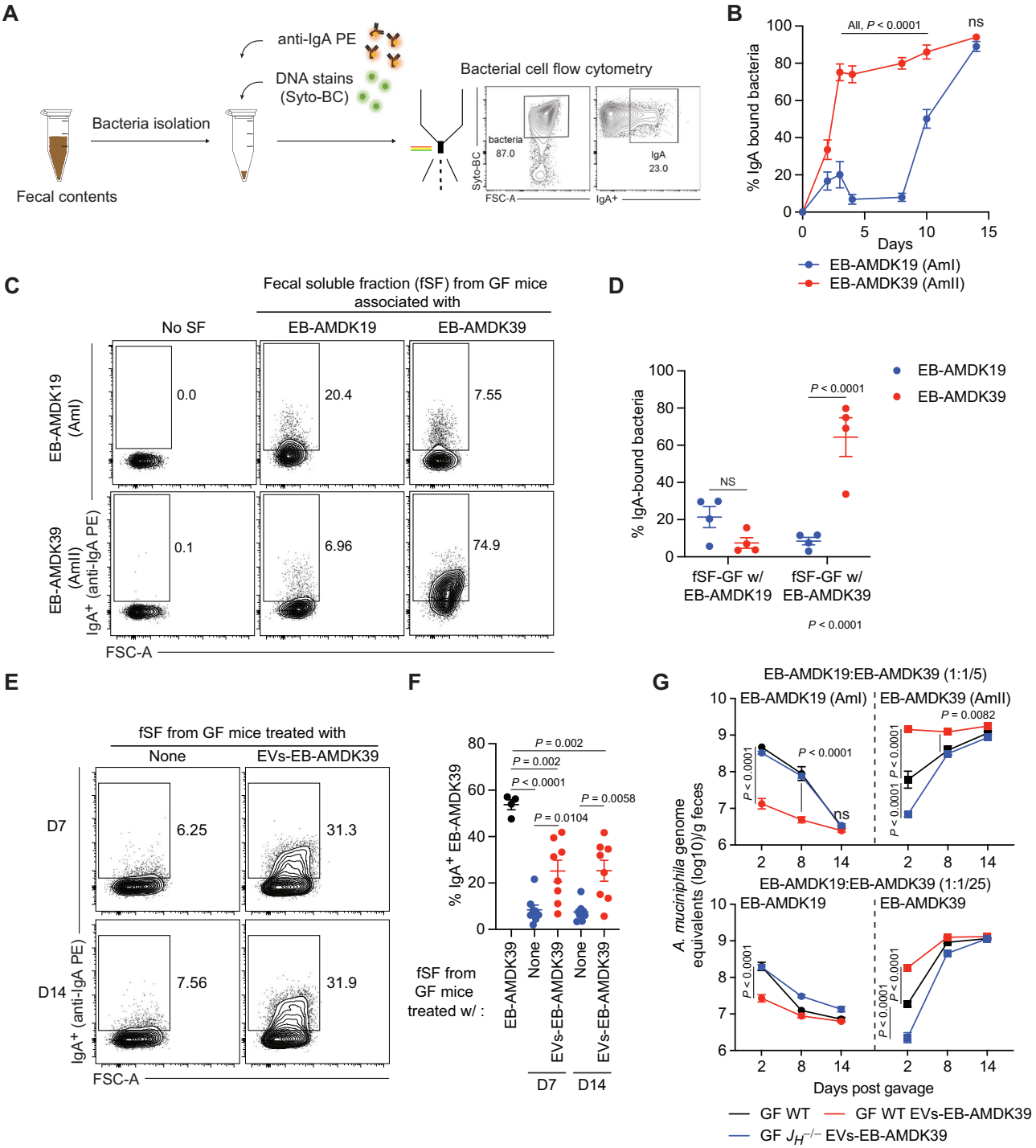

immune responses, particularly focusing on clade-specific IgA production.

Using bacterial cell flow cytometric analysis (Fig. 6A), the proportions of IgA-bound bacteria in the gut of GF mice mono-associated with each *A. muciniphila* clade were examined. IgA-bound bacteria increased over time following colonization (Fig. 6B). Notably, EB-AMDK39 (AmII) induced luminal IgA responses rapidly than EB-AMDK19 (AmI). By day 14 post-colonization, a majority of *A. muciniphila* were bound by IgA, irrespective of clade. Fecal SFs from EB-AMDK19- and EB-AMDK39-associated GF mice were then analyzed for cross-reactivity of clade-induced IgA (Fig. 6C, D). IgAs from EB-AMDK19-associated GF mice showed stronger binding to EB-AMDK19 than to EB-AMDK39 (21.4 ± 11.4% vs 7.5 ± 5.7%), while IgAs from EB-AMDK39-associated GF mice more specifically bound to EB-AMDK39 (64.4 ± 20.9%) than to EB-AMDK19 (8.5 ± 4.1%) (Fig. 6C, D). The results suggest that each *A. muciniphila* clade induces clade-specific IgA responses.

As bacterial EVs can elicit IgA responses under various conditions[51,52], we examined whether AmII-specific IgAs could be induced through oral-administration of AmII-derived EVs in GF mice, and whether these EV-induced IgAs confer competitive advantages against AmI. Fecal SF obtained after oral administration of enriched EB-AMDK39-derived EVs were used to identify AmII-specific IgA. Treatment with enriched EB-AMDK39-derived EVs induced specific IgAs against EB-AMDK39, albeit at a lower level than that of EB-AMDK39-associated GF mice, but still significantly higher than that of GF mice (Fig. 6E, F).

Fig. 6 | EV-induced clade-specific IgA enhances initial colonization of AmII in the host gut. A Schematics of strategies for bacterial cell flow cytometry to examine the proportion of IgA-bound bacteria. **B** Proportions of IgA bound bacteria in GF mice mono-associated with EB-AMDK19 (AmI) and EB-AMDK39 (AmII) ($n = 4$ per group). Each data point represents the average of measurements taken from an individual mouse. **C**, **D** Cross-reactivity of luminal IgAs induced by each clade. Fecal soluble fraction (fSF) obtained from EB-AMDK19- and EB-ADMK39-associated GF mice ($n = 4$ per group). fSF from an individual mouse was used to treat EB-AMDK19 and EB-AMDK39 bacteria and the proportion of IgA bound bacteria was determined by bacterial cell flow cytometry. **C** Representative contour plot showing the proportion of IgA-bound bacteria gated on DNA-stained bacteria. **D** Percentage of IgA-bound bacteria (EB-AMDK19 or EB-AMDK39). Data points represent individual mice. **E**, **F** GF mice were orally treated with enriched EB-AMDK39-derived EVs. At indicated time points, fecal soluble fractions were obtained to examine specific binding to EB-AMDK39 bacteria by bacterial flow cytometry ($n = 4$ for GF mice associated with EB-AMDK39, $n = 8$ for untreated GF mice and GF mice orally treated with enriched EB-AMDK39-derived EVs). **E** Representative plot showing the proportion of IgA-bound EB-AMDK39 gated on DNA-stained bacteria. **F** Percentage of IgA-bound EB-AMDK39. **G** Effect of IgAs induced by oral administration of enriched EB-AMDK39-derived EV on the initial colonization of EB-AMDK39. GF wildtype (WT) mice, GF WT mice, and B cell-deficient $J_H^{-/-}$ mice treated with enriched EB-AMDK39-derived EVs (50 μg per mouse) were administered with a mixture of EB-AMDK19 (1×10^8 CFU per mouse) and EB-AMDK39 (2×10^7 CFU or 4×10^6 CFU) on day 14 post-EV administration. GF WT mice without EV administration were used as a negative control ($n = 4$ per group). The level of each clade in feces was quantified by qPCR with clade-specific primers. Each point represents the average of measurements taken from an individual mouse. Statistical differences were determined by two-way ANOVA with Sidak's multiple comparison tests (**B**, **D**, **G**) or by one-way ANOVA with Tukey's multiple comparisons test (**F**). ns: not significant. Error bars represent SEM. Source data are provided as a Source Data file.

Next, to assess whether AmII-specific IgA influences competitive exclusion between *A. muciniphila* clades, we orally treated GF mice with enriched EB-AMDK39-derived EVs before introducing a mixture of EB-AMDK19 and EB-AMDK39. As EB-AMDK39 predominated under equal co-administration, the effect of EV-induced IgAs was investigated by lowering the ratio of EB-AMDK39 to 1/5th or 1/25th of EB-AMDK19. Pre-treatment of enriched EB-AMDK39-derived EVs boosted EB-AMDK39 levels significantly, enabling it to outcompete EB-AMDK19 by day 2 post co-administration. Conversely, in GF mice without EV pre-treatment, EB-AMDK19 levels surged above those of EB-AMDK39 (Fig. 6G).

To further clarify whether pre-administration of AmII-derived EVs drive AmII predominance via IgA induction, we compared the outcomes in GF $J_H^{-/-}$ mice lacking B cells. In these mice, pre-treatment of enriched EB-AMDK39-derived EVs failed to confer a competitive advantage to EB-AMDK39 over EB-AMDK19 by day 2 post co-administration (Fig. 6G). These results support the idea that the effect of EVs pre-treatment on competition between two clades is dependent on clade-specific IgA responses. By day 14, however, EB-AMDK39 outcompeted EB-AMDK19 regardless of EV pre-treatment, suggesting that the inherent competitive advantage of AmII persists, even at lower initial ratios. Overall, these results suggest that AmII-derived EVs not only facilitate inter-clade competition by inhibiting AmI growth but also engage the host immune system to produce AmII-specific IgA, which enhances the colonization of AmII.

Discussion

Genomic divergence at the sub-species level during host adaptation and evolution leads to phenotypic variations that influence inter-species and host-microbe interactions significantly[53–55]. Identifying gut microbes at the sub-species level, particularly *A. muciniphila*, in which single clade predominates within an individual host, is critical for understanding their roles in health and disease. Here, evolutionary divergence was observed among human-associated *A. muciniphila* using the Genome Taxonomy Database, revealing distinct evolutionary patterns (Supplementary Fig. 11). Despite the low pairwise sequence distance of the 16S rRNA gene (< 2%), whole-genome comparisons indicated substantial divergence (> 12%) (Supplementary Fig. 1 and Supplementary Table 1), likely driven by rapid genomic diversification within humans. The low sequence divergence of 16S rRNA gene complicates the identification of *A. muciniphila* clades through 16S rRNA operational taxonomic unit (OTU) clustering.

The application of ASV analysis, therefore, is essential in uncovering sub-species diversity and *A. muciniphila* clade population structure[56–58]. By leveraging the high-resolution power of ASVs, we successfully typed *A. muciniphila* clades simply using 16S rRNA amplicon sequencing data. The approach proved useful in understanding *A. muciniphila* diversity in Korean subjects, and could be extended to investigate the global distribution of *A. muciniphila* clades. We found that *A. muciniphila* diversity can be influenced by urbanization and a single clade predominance is a widespread feature across different human populations. Notably, a strong correlation was observed between urbanization rates and the prevalence of certain clades, such as AmII and AmIV. The findings suggest that environmental factors, including diet and lifestyle associated with industrialization, impact *A. muciniphila* clade distribution significantly. The findings also open new avenues for investigating how modern lifestyles and dietary habits may shape gut microbiota composition at a fine taxonomic level.

It remains unclear whether individuals with distinct *A. muciniphila* clades might experience different health outcomes. In our dataset of 890 healthy Koreans, no significant physiological differences were observed based on *A. muciniphila* clade, suggesting no severe health impacts associated with clade variation in healthy individuals. However, it is plausible that health outcomes could differ depending on the *A. muciniphila* clade in disease contexts, such as obesity and cancer. Future studies aimed at elucidating the specific environmental factors affecting *A. muciniphila* diversity and the correlations between its clades and health outcomes will be crucial, not only for deeper understanding of how the gut microbes impact health and disease at the sub-species level but also for developing *A. muciniphila*-targeted therapeutic interventions.

A. muciniphila can establish collateral commensalism with other microbial species, and the interaction, particularly with species such as *Eubacterium hallii*, enhances responses to immune checkpoint blockade in tumor patients significantly[12]. The microbial species that correlate with *A. muciniphila* may vary depending on the clade. While addressing this issue is beyond the scope of the present study, significant differences in gut microbial composition were observed according to *A. muciniphila* clades in healthy Korean subjects (PERMANOVA, $p = 0.028$) (Supplementary Fig. 12A, B). The core ASVs correlated with *A. muciniphila* differed by clade, suggesting that the microbial species with which *A. muciniphila* symbiotically interact may vary between clades (Supplementary Fig. 12C). The ASV-based analysis further supports the possibility that *A. muciniphila* may influence health outcomes depending on clade by inducing compositional changes in gut microbiota.

AmI clades possess genes involved in the assimilatory sulfate reduction, specifically related to mucin utilization, some of which are absent in AmII (Supplementary Data 2, 3). In contrast, AmI lacks certain capabilities, such as vitamin B12 synthesis, which are retained in AmII (Supplementary Data 2)[14]. This suggests that *A. muciniphila* clades may have adapted to occupy ecological niches within the gut via different colonization strategies. A possible scenario for AmI involves undergoing genetic changes to enhance mucin utilization for host adaptation while relying on syntrophic interactions with other microbial species for essential nutrients such as vitamin B12[59]. Considerable proportions of individuals bearing AmII clade, especially in urban

populations, suggest that AmII clade may have evolved to possess a competitive advantage over AmI. We propose that AmII gains a competitive advantage by producing EVs with inhibitory effects on AmI growth, surpassing AmI's superior capacity for mucin utilization. While AmII-derived EVs directly mediate AmI growth inhibition, these EVs also stimulate host immune responses to produce AmII-specific IgA. Although clade-specific IgA is not a decisive factor for AmII predominance, it could facilitate the mucosal colonization of AmII. The findings underscore the importance of understanding the immune modulatory properties of gut microbes at the sub-species or clade levels to unravel the immune–microbe interactions. Exploring how host immunity can be modulated to enhance mucosal colonization of *A. muciniphila* could facilitate development of effective therapeutic intervention strategies.

However, the widespread prevalence of AmI in human populations suggests that competition between clades is not determined solely by the unilateral inhibitory effects of AmII-derived EVs. Factors such as the pre-occupancy effect, where early colonization may confer advantages that override subsequent competitive pressures, appear to play a significant role in shaping a clade predominance in human populations. Moreover, the inhibitory effect mediated by AmII-derived EVs exhibits a specific threshold, suggesting that a balance between inter-clade inhibition mediated by AmII-derived EVs and pre-occupancy effect, affected by colonization timing, contribute to the overall composition of *A. muciniphila* in the host gut.

The exact mechanism via which AmII-derived EVs inhibit AmI growth remains unclear. Interestingly, proteomic profiling between AmII-derived whole cell lysates and EVs revealed that AmII-derived EVs are enriched with Rhs repeat proteins which are associated with inter-bacterial competition[46,47]. While it is possible that Rhs repeat proteins of AmII, delivered via EVs, contribute to unilateral inhibition of AmI growth, direct experimental evidence supporting this mechanism is currently lacking. However, several observations make this hypothesis worth further investigation. First, EVs, such as OMVs produced by Gram-negative bacteria, can carry proteolytic enzymes that mediate the killing of microbial prey[27,31]. Second, Rhs repeat proteins promote bacterial diversity and evolution by enabling bacteria to outcompete and eliminate neighboring rivals in resource-limited environments[46,47]. Although limited to AmI, Rhs repeat proteins have likely exerted selective pressure during *A. muciniphila* evolution[60]. Third, comparative genomic analysis revealed that AmII strains express unique Rhs repeat proteins not found in AmI strains, permitting unilateral inhibition. Fourth, bacteria can produce immunity Rhs protein that neutralize their own Rhs-CT toxins, allowing for selective targeting of competitors[46,47]. Future studies using targeted mutations of Rhs repeat proteins in *A. muciniphila* will be needed to clarify whether these proteins directly contribute to the competitive exclusion of AmI by AmII.

In conclusion, the widespread predominance of a single *A. muciniphila* clade is driven by the evolutionary diversification of inter-clade competition strategies. Specifically, the AmII clade exhibits a competitive advantage by producing EVs that not only inhibit the AmI growth directly but also promote AmII clade colonization by inducing IgAs. These AmII-derived EVs effectively counteract AmI clade's enhanced capacity for mucin utilization. Our findings underscore the importance of understanding the diversification of *A. muciniphila* and its interactions with the host immune system, providing valuable insights for harnessing its therapeutic potential for the treatment of metabolic disorders and enhancing anti-tumor immunotherapy.

Methods

A. muciniphila clade ASV and 16S amplicon data collection and analysis

To examine the population-level distribution of *A. muciniphila* clades, we first utilized the 16S rRNA gene sequencing data from our previous study that characterized the microbiomes of 890 healthy Korean individuals[39]. The 16S rRNA gene sequencing data were processed into an ASV frequency table using the DADA2 pipeline of QIIME2 (v2022.02) (https://qiime2.org/). Taxonomical classifications were annotated to the ASVs using the scikit-learn naive Bayes machine-learning classifier and the Silva v138 database[61]. To classify the ASVs into *A. muciniphila* clades, 92 complete human-associated *A. muciniphila* genomes were transformed into a BLAST database using the BLAST+ package. Each ASV sequence was queried in the database using BLAST (v2.9.0 +) (https://blast.ncbi.nlm.nih.gov/Blast.cgi). The corresponding clades of the retrieved genomes were assigned to the ASVs (perfect matches). For global clade distribution analysis, 16S rRNA gene sequencing data were collected from 21 other countries, targeting the V3–V4 or V4 region with the Illumina sequencing platform (Supplementary Data 4)[62–84]. Only healthy adult samples, such as control groups or pre-intervention samples, were included. The ASV generation and clade classification methods were consistent with those used for the Korean data. Urban rates for each country were sourced from the world urbanization prospects published by the United Nations[85]. Map image created using R packages maps v3.4.1. and ggplot2 v3.4.0.

In vitro *A. muciniphila* co-culture test

Changes in the relative abundance of each *A. muciniphila* clade were examined after co-inoculation with both clades. Equal numbers of AmI and AmII representative strains, EB-AMDK19 and EB-AMDK39, respectively, were co-inoculated into the culture media (30 g/L of tryptic soy broth, 2.5 g/L of mucin from porcine stomach, 0.1 mg/L of cyanocobalamin, and 0.5 g/L of L-cysteine hydrochloride) in an anaerobic chamber filled with 90% N_2, 5% CO_2, and 5% H_2 at 37 °C. Single clade inoculation served as controls. Bacteria pellets were harvested at 24 and 48 h post-inoculation by centrifugation (10,000 × *g* for 10 min at 4 °C). To monitor the levels of live bacteria belonging to each clade, total RNA was extracted using an RNA extraction kit (TaKaRa MiniBEST Universal RNA Extraction Kit, Dalian, China). Total RNA (100 ng) was reverse-transcribed into cDNA using an M-MLV cDNA synthesis kit (Enzynomics, Daejeon, South Korea), and relative expression of clade specific genes was examined by quantitative PCR (qPCR) using a quantitative PCR kit (TOPreal SYBR Green High-ROX PreMIX, Enzynomics) and the CFX96TM real-time system (Bio-Rad, Hercules, CA, USA). Information on the clade-specific primers is listed in Supplementary Data 6. Ct values were normalized to those of the 16S rRNA gene as an internal control, and relative gene expression was calculated using the $2^{-\Delta\Delta Ct}$ method.

To examine changes in the relative abundance of *A. muciniphila* clades upon addition of EB-AMDK39 (AmII) to EB-AMDK19 (AmI)-enriched culture, EB-AMDK19 was first inoculated into the culture media under anaerobic conditions at 37 °C. At 24–48 h post-incubation, EB-AMDK39 (1×10^8 CFU) was additionally inoculated into the EB-AMDK19-enriched culture (1×10^{10} CFU/culture). Single inoculation of each *A. muciniphila* clade was used as the control for the relative abundance of each clade. Furthermore, the relative abundance of each *A. muciniphila* clade was analyzed as explained above.

In vitro test for cross-clade growth inhibition of *A. muciniphila* via cell culture supernatants

Cell-free culture supernatants derived from each clade were tested for their effects on the growth of the other. AmI and AmII strains were inoculated into the mucin-based media (30 g/L of tryptic soy broth, 2.5 g/L of mucin from porcine stomach, 0.1 mg/L of cyanocobalamin, and 0.5 g/L of L-cysteine hydrochloride) under anaerobic conditions (90% N_2, 5% CO_2, and 5% H_2) at 37 °C. After 24 h, when the cultures had reached stationary phase, culture supernatants were separated by centrifugation (10,000 × *g* for 10 min at 4 °C) and filtered through a 0.2 μm syringe filter. The supernatants (20% v/v) were then added to fresh cultures of *A. muciniphila* strains (1×10^6 CFU/culture). Growth inhibition was assessed by absorbance after 24 h, compared with

untreated controls. Heat treatment (95 °C for 15 min) was also tested for its effect on inhibitory activity of culture supernatants. To assess the effect of proteinase K treatment, supernatants were treated with proteinase K (1 mg/mL, iNtRON Biotechnology, Seoul, Korea) for 16 h at 37 °C and protease inhibitor (Sigma-Aldrich, St. Louis, MO, USA) was added (1 mM). To estimate the molecular weight of the inhibitory substances present in AmII-derived supernatants, the supernatants were passed through Amicon Ultra centrifugal filters with cut-off sizes of 10, 30 and 100 kDa (Sigma-Aldrich, St. Louis, MO, USA). The effect on AmI growth was assessed by comparing the absorbance value after 48 h.

Test for ASR gene expression by *A. muciniphila* strains and influence of L-cysteine depletion on *A. muciniphila* growth in vitro

The distribution of assimilatory sulfate reduction (ASR) genes among *A. muciniphila* clades was assessed using BAA-835 as a reference to identify homologs in other *A. muciniphila* strains[15]. To examine each ASR gene in various *A. muciniphila* strains, AmI and AmII strains were inoculated into a mucin-based medium as described above. After 48 h, total RNA was extracted and cDNA was prepared for qPCR. The primer sequences for each ASR gene are listed in Supplementary Data 6. To further examine the effect of ASR genes on mucin utilization, AmI and AmII strains were inoculated into the mucin-based medium with or without L-cysteine (0.5 g/L) and cultured under anaerobic conditions at 37 °C. The effect of L-cysteine on growth was assessed by comparing the absorbance value after 48 h.

In vitro test to examine mucin-free AmII supernatants for AmI growth inhibition

To examine whether biotic components from the porcine mucus in AmII-derived supernatants contribute to AmI growth inhibition, AmII-derived supernatants were prepared under mucin free conditions. Specifically, EB-AMDK39 (AmII) strain was inoculated into two types of mucin-free medium, either a glucosamine-based medium (30 g/L of tryptic soy broth, 2.5 g/L N-acetyl-D-glucosamine, 2.5 g/L D-lactose, 4.0 g/L L-Threonine, 0.1 mg/L of cyanocobalamin, and 0.5 g/L of L-cysteine hydrochloride) or a soy-peptone-based medium (20 g/L soy-peptone, 10 g/L yeast extract, 2.5 g/L K2HPO4, 2.5 g/L KH2PO4, 5 g/L N-acetyl-D-glucosamine, 5 g/L D-lactose, 2.5 g/L D-fructose, 8 g/L L-aspartic acid, 0.1 mg/L cyanocobalamin, and 0.5 g/L L-cysteine hydrochloride). Supernatants derived from the media (20%, v/v) were applied to fresh cultures of EB-AMDK19 (AmI) in three different media and the effect on the AmI growth was examined as described earlier.

Size exclusion chromatography

A. muciniphila was cultured in mucin-free soy-peptone-based medium (20 g/L soy-peptone, 10 g/L yeast extract, 2.5 g/L K2HPO4, 2.5 g/L KH2PO4, 5 g/L N-acetyl-D-glucosamine, 5 g/L D-lactose, 2.5 g/L D-fructose, 8 g/L L-aspartic acid, 0.1 mg/L cyanocobalamin, and 0.5 g/L L-cysteine hydrochloride) in an anaerobic chamber filled with 90% N_2, 5% CO_2, and 5% H_2 at 37 °C. *A. muciniphila*-derived cell-free supernatants were concentrated using Ultra-15 30 kDa Amicon centrifugal filter units to a final volume of 500 μL. For further purification of EVs, the filtrate was subjected to size-exclusion chromatography; 500 μL of filtrate was loaded onto a column filled with Sepharose CL-6B resin in a 10-mL bed volume. Subsequently, samples were fractionated into 50 samples of 0.25 mL each. Phosphate-buffered saline (PBS) was used as the mobile phase. To test the inhibitory effect of fractions, the obtained fractions were treated with 10% (v/v) conditions when inoculating EB-AMDK19 and EB-AMDK39 into the culture medium.

Preparation of *A. muciniphila*-derived EVs

To prepare enriched *A. muciniphila*-derived EVs, the supernatant was filtered through a 0.22 μm vacuum filter and concentrated using a 500 kDa hollow fiber membrane mounted on a QuixStand benchtop system (GE Healthcare, Little Chalfont, UK). The resulting supernatant was then precipitated using differential centrifugation methods. Specifically, the sample was centrifuged at 80,000 × *g* for 1 h at 4 °C, and the resulting supernatant was centrifuged further at 150,000 × *g* for 3 h at 4 °C, and the pellet was resuspended in 20 mM Tris-HCl buffer (pH 8.0). The protein concentration of each sample was determined using a micro BCA protein assay kit (Thermo Fisher Scientific, Waltham, MA, USA) according to the manufacturer's instructions. Finally, the samples were aliquoted and stored at −80 °C until further use.

Nanoparticle tracking analysis

Nanoparticle tracking analysis (NTA) was performed using a NanoSight NS300 (Malvern Panalytical, Westborough, MA, USA) device to confirm the concentration (particles/mL) of EVs (NTA 3.4 Build 3.4.003). In the NTA, a CCD camera with a slider shutter speed of 1500 a slider gain of 680, at 30.0 frames/s, and the number of frames was 2700. Samples were collected and diluted to perform NTA.

Disk diffusion test

Each *A. muciniphila* strain (EB-AMDK19 or EB-AMDK39) was spread onto the tryptic soy broth containing mucin (TSBM) agar plate (30 g/L of tryptic soy broth, 2.5 g/L of mucin from porcine stomach, 0.1 mg/L of cyanocobalamin, and 0.5 g/L of L-cysteine hydrochloride, and 14 g/L agar). Then, sterilized and dried filter paper disks were placed on the agar plate. At 24 h post-incubation under anaerobic conditions, 10 μL of EV-containing samples, such as enriched EB-AMDK39 (AmII)-derived EVs or whole soluble fractions from EB-AMDK39-associated GF mice, was dropped onto the filter paper disks, and the plates were incubated for 24–48 h.

Transmission electron microscopy

A drop of a sample was placed on discharged formvar/carbon-coated grids for 5 min and rinsed three times with deionized water. After a single wash with distilled water, negative staining was then performed with three consecutive contrasting steps using 1% uranyl acetate. Dried grids were used to observe images through TEM (JEM-2100F, JEOL, Tokyo, Japan) at an acceleration voltage of 200 kV with a Megaview III CCD camera.

Protein sample preparation and proteomic analysis using LC-MS/MS

Two subcellular fractions, WCLs and EVs, were prepared from *A. muciniphila*. To obtain the fractions, 1 L of bacterial culture was harvested through centrifugation at 10,000 × *g* for 20 min at 4 °C to remove cell debris. The resulting supernatant and pellet fractions were separated and subjected to further processing. The WCL was washed thrice with 20 mM Tris-HCl buffer (pH 8.0) and then disrupted using a French pressure cell (SLM Aminco, Urbana, IL, USA) at 138 MPa until a transparent solution was obtained.

To conduct label-free proteomics, in-gel digestion was performed. The eluents were analyzed through LC-MS/MS using Orbitrap Q Exactive Plus (Thermo Fisher Scientific). The MaxQuant platform was used for label-free quantification (LFQ) analysis. Briefly, LFQ represents the normalized intensity of proteins, allowing comparison across samples without labeling techniques[86]. The genome of *A. muciniphila* (NCBI, CP029753.1, 2542 sequences, date of release: February 6, 2020) was used as a reference genome. The following parameters were used for protein identification: missed cleavages, 2; peptide mass tolerance, ±10 ppm; peptide fragment tolerance, ±0.8 Da; peptide charge, 2+, 3+, and 4+; static modifications (carbamidomethyl); and dynamic modification (oxidation (Met)). A target-decoy search was employed to remove the low-confidence peptides and proteins with a false discovery rate of at least 1%. To reduce the number of false positives, proteins identified more than twice in the

three replicates were considered positive in the dataset. The differentially expressed proteins (DEPs) were selected using the Limma package in R (version 4.3), which employs an empirical Bayes approach to improve variance estimation in small-sample proteomic datasets. A moderated two-sided t-test was performed, and multiple testing correction was applied using the Benjamini-Hochberg method to control the false discovery rate. Functional annotations of DEPs were analyzed using GSEA-Pro v.3 (http://gseapro.molgenrug.nl/).

Mice

GF C57BL/6 N (B6) and $J_H^{-/-}$ mice were kindly provided by Dr. Andrew Macpherson (Bern University, Switzerland) and maintained in sterile flexible film isolators (Class Biological Clean Ltd., Madison, WI, USA) under a standard 12-hour light/dark cycle and given autoclaved Teklad Global 18% Protein Rodent Diet (2018S, Envigo, USA) *ad libitum*. Age- and sex-matched 6– to 8-week-old mice bred in the animal facility of the POSTECH Biotech Center were used for all experiments. All animal studies were performed in accordance with the guidelines of the Institutional Animal Care and Use Committee of POSTECH (approval no. POSTECH-2023-0045 and POSTECH-2024-0090). GF mice were routinely monitored for microbial contamination by culturing fresh fecal samples in aerobic and anaerobic conditions.

Colonization of *A. muciniphila* strains into GF mice and ASF gnotobiotic mice

GF C57BL/6 (B6) mice were used to examine co-exclusion between *A. muciniphila* clades. For colonization of *A. muciniphila* into GF mice, a tightly-sealed frozen stock vial containing each *A. muciniphila* clade was imported into flexible film isolators. For mono-association, 1×10^8 CFU of *A. muciniphila* were administrated orally into GF mice. For association of multiple *A. muciniphila* strains, tightly-sealed frozen stock vials each containing an *A. muciniphila* strain were imported, equally mixed inside flexible film isolators using syringes, and then administrated orally into GF mice or gnotobiotic B6 mice colonized with Altered Schaedler's flora, a consortium of eight different anaerobic bacteria (1×10^8 CFU per *A. muciniphila* strain)[87]. To produce ASF gnotobiotic mice, NOD.SCID mice harboring ASF were purchased from Taconic Biosciences and co-housed with GF B6 mice. Feces were harvested from the co-housed GF B6 mice and used for producing ASF gnotobiotic mice. To test the pre-occupancy effect on competitive exclusion between different clades, GF mice were first gavaged with 1×10^8 CFU of EB-AMDK39 (AmII) or EB-AMDK19 (AmII) and then at day 19 post-administration, EB-AMDK19 or EB-AMDK39 were gavaged, respectively.

Determination of luminal levels of *A. muciniphila* and ASF strains in gnotobiotic mice

To determine luminal levels of *A. muciniphila*, fresh fecal samples were collected at various time points from GF or ASF gnotobiotic mice associated with either single or multiple strains of *A. muciniphila*. Fecal genomic DNA was extracted using a fecal DNA extraction kit (QIAamp PowerFecal pro DNA kit, Qiagen) for each experimental group. qPCR was conducted with species-, clade- or strain-specific primers for *A. muciniphila*, using a quantitative PCR kit (TOPreal SYBR Green High-ROX PreMIX, Enzynomics). To assess luminal levels of ASF bacteria, qPCR was conducted using fecal genomic DNA from ASF gnotobiotic mice associated with *A. muciniphila*, as described above[87]. Primer sequences are listed in Supplementary Data 6. The PCR conditions were as follows: 40 cycles at 50 °C for 4 min, 95 °C for 10 min, 95 °C for 30 s, and 56 °C for 30 s.

EVs isolation from fecal samples

Frozen feces (0.5 g; stored at −80 °C for less than 2 weeks) obtained from GF mice or AmII-colonized mice were dissolved in 10 ml filtered PBS. Two rounds of centrifugation were applied (3000 × *g* for 15 min at 4 °C) to remove solid debris. After centrifugation, the fecal SF was filtered through two filters with different pore sizes consecutively: 0.45 µm and 0.2 µm (Minisart, Sartorius AG, Goettingen, Germany). Vesicles were concentrated by loading the original flow through onto a filter with a molecular weight cut-off of 30 kDa (Amicon Ultra 15 ml Centrifugal Filter Unit, Merck Millipore, Billerica, MA, USA). The filter membrane was rinsed with 250 µl sterile PBS, and an end volume of 500 µl was used for the size-exclusion chromatography. The concentrate was purified using size-exclusion chromatography with 10 mL CL-6B Sepharose columns (GE Healthcare, Eindhoven, the Netherlands). The concentrated supernatant was loaded onto the column, and 0.5 mL of fractions was immediately collected in sterilized tubes. In total, 0.25 mL of 50 fractions was collected per sample. To test the inhibitory effect of fractions, the obtained fractions were treated under 10% (v/v) conditions when inoculating EB-AMDK19 and EB-AMDK39 into the culture medium.

Experiments with enriched EVs-administrated GF mice

To assess the induction of EB-AMDK39-specific IgA by the oral administration of enriched EB-AMDK39-derived EVs and its effect on the EB-AMDK39 colonization, GF B6 and $J_H^{-/-}$ mice were administrated orally with 50 µg of enriched EB-AMDK39-derived EVs two times on day 0 and 4. Feces were collected on days 7 and 14 to examine the induction of EB-AMDK39-specific IgA. On day 14, EV-administrated GF mice were colonized with mixtures of EB-AMDK19 (10^8 CFU per mouse) and EB-AMDK39 ($1/5^{th}$ or $1/25^{th}$ of EB-AMDK19 per mouse). Fresh fecal samples were collected at different time points to examine luminal levels of each strain using qPCR with clade-specific primers.

Bacterial flow cytometry

For fecal bacterial isolation, fecal pellets were resuspended at 100 mg/mL in sterile PBS and homogenized. The samples were centrifuged at 400 × g for 5 min at 4 °C, and the supernatant was transferred into a new tube to remove solid debris; the process was repeated twice. The supernatant was centrifuged at 8000 × g for 10 min at 4 °C to pellet bacteria. Supernatant containing soluble antibodies was transferred into a new tube and stored at −80 °C for in vitro bacteria cross-reactivity assay. Bacterial pellets were resuspended in sterile PBS containing bovine serum albumin (1% v/v). Fecal bacteria isolates were stained with the following fluorochrome-conjugated antibodies: at 1:100 dilution: PE conjugated anti-mouse IgA (Invitrogen, MA, USA, mA-6E1, #12-4204-83) for 30 min at 4 °C in the dark. Samples were washed and resuspended in PBS with 5 mM SYTO-BC, a cell-permeable DNA staining dye (Invitrogen, MA, USA, #34855). Flow cytometry was performed on CytoFLEX LX (Beckman Coulter, Brea, CA, USA) at the Microbiome Core facility of POSTECH and analysis was performed using FlowJo software (Treestar Ashland, OR, USA).

In vitro cross-reactivity assay

Fecal soluble fractions were collected from GF mice mono-associated with EB-AMDK19 and EB-AMDK39 on day 14. Soluble antibodies in 50 µl of fecal soluble fraction was incubated with 1×10^6 CFU of each *A. muciniphila* strain (EB-AMDK19 and EB-AMDK39) at 37 °C for 2 h. After incubation, cross-reactivity was assessed through bacterial flow cytometry.

Clustering and phylogenetic analysis of Rhs repeat proteins

Full set sequences of Rhs repeat proteins, including disordered, repeated, and core domains, were multiple aligned using ClustalOmega with default options (filtered with the minimum length criterion, 1500 aa). Pairwise distance was calculated using the Jones–Tayler–Thornton substitution model and uniform substitution rate through MEGA11 software[88]. Distances were reformed to a similarity matrix, and hierarchical clustering was performed through single-linkage clustering with the number of clusters

restricted to 10. The phylogenetic tree was visualized through Interactive Tree Of Life[89].

Statistical analysis
GraphPad Prism 10 (GraphPad, San Diego, CA, USA) was used for all statistical analyses, including one-way or two-way Analysis of Variance with Turkey's or Sidaak's multiple comparisons tests, respectively. *p*-value lower than 0.05 indicates significance.

Reporting summary
Further information on research design is available in the Nature Portfolio Reporting Summary linked to this article.

Data availability
All data associated with this study are present in the Supplementary Materials. All raw data for the main figures is provided in the Source Data file provided with this paper. Accession codes for 92 human-associated *A. muciniphila* genome data are summarized in Supplementary Data 1. Accession codes for 16S amplicon data collection are summarized in Supplementary Data 4. The mass spectrometry raw data generated in this study have been deposited in the ProteomeXchange database under following accession code: PXD045095 Source data are provided with this paper.

Code availability
No new code was created in this study.

References

1. Wang, B., Yao, M., Lv, L., Ling, Z. & Li, L. The human microbiota in health and disease. *Engineering* **3**, 71–82 (2017).
2. Gomaa, E. Z. Human gut microbiota/microbiome in health and diseases: a review. *Antonie Van. Leeuwenhoek* **113**, 2019–2040 (2020).
3. Cani, P. D. & de Vos, W. M. Next-generation beneficial microbes: the case of Akkermansia muciniphila. *Front. Microbiol.* **8**, 1765 (2017).
4. Zhang, T., Li, Q., Cheng, L., Buch, H. & Zhang, F. Akkermansia muciniphila is a promising probiotic. *Microb. Biotechnol.* **12**, 1109–1125 (2019).
5. Derrien, M., Belzer, C. & de Vos, W. M. Akkermansia muciniphila and its role in regulating host functions. *Microb. Pathogenesis* **106**, 171–181 (2017).
6. Zhao, Q. et al. Akkermansia muciniphila plays critical roles in host health. *Crit. Rev. Microbiol.* **49**, 82–100 (2023).
7. Yoon, H. S. et al. Akkermansia muciniphila secretes a glucagon-like peptide-1-inducing protein that improves glucose homeostasis and ameliorates metabolic disease in mice. *Nat. Microbiol.* **6**, 563–573 (2021).
8. Depommier, C. et al. Supplementation with Akkermansia muciniphila in overweight and obese human volunteers: a proof-of-concept exploratory study. *Nat. Med.* **25**, 1096–1103 (2019).
9. Everard, A. et al. Cross-talk between Akkermansia muciniphila and intestinal epithelium controls diet-induced obesity. *Proc. Natl Acad. Sci. USA* **110**, 9066–9071 (2013).
10. Chelakkot, C. et al. Akkermansia muciniphila-derived extracellular vesicles influence gut permeability through the regulation of tight junctions. *Exp. Mol. Med.* **50**, e450–e450 (2018).
11. Routy, B. et al. Gut microbiome influences efficacy of PD-1–based immunotherapy against epithelial tumors. *Science* **359**, 91–97 (2018).
12. Derosa, L. et al. Intestinal Akkermansia muciniphila predicts clinical response to PD-1 blockade in patients with advanced non-small-cell lung cancer. *Nat. Med.* **28**, 315–324 (2022).
13. Guo, X. et al. Genome sequencing of 39 Akkermansia muciniphila isolates reveals its population structure, genomic and functional diversity, and global distribution in mammalian gut microbiotas. *BMC genomics* **18**, 1–12 (2017).
14. Kirmiz, N. et al. Comparative genomics guides elucidation of vitamin B12 biosynthesis in novel human-associated Akkermansia strains. *Appl. Environ. Microbiol.* **86**, e02117–02119 (2020).
15. Becken, B. et al. Genotypic and phenotypic diversity among human isolates of Akkermansia muciniphila. *Mbio* **12**, 00478–00421 (2021).
16. Ndongo, S., Armstrong, N., Raoult, D. & Fournier, P.-E. Reclassification of eight Akkermansia muciniphila strains and description of Akkermansia massiliensis sp. nov. and Candidatus Akkermansia timonensis, isolated from human feces. *Sci. Rep.* **12**, 21747 (2022).
17. Kumar, R. et al. Identification and characterization of a novel species of genus Akkermansia with metabolic health effects in a diet-induced obesity mouse model. *Cells* **11**, 2084 (2022).
18. Kobayashi, Y., Kawahara, T., Inoue, S. & Kohda, N. Akkermansia biwaensis sp. nov., an anaerobic mucin-degrading bacterium isolated from human faeces. *Int. J. Syst. Evolut. Microbiol.* **73**, 005697 (2023).
19. De Filippis, F. et al. Distinct genetic and functional traits of human intestinal Prevotella copri strains are associated with different habitual diets. *Cell host microbe* **25**, 444–453. e443 (2019).
20. Yang, C. et al. Fecal IgA levels are determined by strain-level differences in Bacteroides ovatus and are modifiable by gut microbiota manipulation. *Cell host microbe* **27**, 467–475. e466 (2020).
21. Liu, M.-J. et al. Recent findings in Akkermansia muciniphila-regulated metabolism and its role in intestinal diseases. *Clin. Nutr.* **41**, 2333–2344 (2022).
22. Geerlings, S. Y., Kostopoulos, I., De Vos, W. M. & Belzer, C. Akkermansia muciniphila in the human gastrointestinal tract: when, where, and how? *Microorganisms* **6**, 75 (2018).
23. Zhou, K. Strategies to promote abundance of Akkermansia muciniphila, an emerging probiotics in the gut, evidence from dietary intervention studies. *J. Funct. foods* **33**, 194–201 (2017).
24. Derrien, M. et al. Modulation of mucosal immune response, tolerance, and proliferation in mice colonized by the mucin-degrader Akkermansia muciniphila. *Front. Microbiol.* **2**, 166 (2011).
25. Van Herreweghen, F. et al. In vitro colonisation of the distal colon by Akkermansia muciniphila is largely mucin and pH dependent. *Beneficial microbes* **8**, 81–96 (2017).
26. Karcher, N. et al. Genomic diversity and ecology of human-associated Akkermansia species in the gut microbiome revealed by extensive metagenomic assembly. *Genome Biol.* **22**, 209 (2021).
27. Schwechheimer, C. & Kuehn, M. J. Outer-membrane vesicles from Gram-negative bacteria: biogenesis and functions. *Nat. Rev. Microbiol* **13**, 605–619 (2015).
28. McMillan, H. M. & Kuehn, M. J. The extracellular vesicle generation paradox: a bacterial point of view. *EMBO J.* **40**, e108174 (2021).
29. Toyofuku, M., Schild, S., Kaparakis-Liaskos, M. & Eberl, L. Composition and functions of bacterial membrane vesicles. *Nat. Rev. Microbiol* **21**, 415–430 (2023).
30. Kadurugamuwa, J. L. & Beveridge, T. J. Bacteriolytic effect of membrane vesicles from Pseudomonas aeruginosa on other bacteria including pathogens: conceptually new antibiotics. *J. Bacteriol.* **178**, 2767–2774 (1996).
31. Berleman, J. E. et al. The lethal cargo of Myxococcus xanthus outer membrane vesicles. *Front Microbiol* **5**, 474 (2014).
32. Emerson, L. E. et al. Extracellular vesicles elicit protective immune responses against Salmonella infection. *J. Extracell. Vesicles* **11**, e12267 (2022).
33. Díez-Sainz, E., Milagro, F. I., Riezu-Boj, J. I. & Lorente-Cebrian, S. Effects of gut microbiota–derived extracellular vesicles on obesity and diabetes and their potential modulation through diet. *J. Physiol. Biochem.* **78**, 1–15 (2021).

34. Ashrafian, F. et al. Akkermansia muciniphila-derived extracellular vesicles as a mucosal delivery vector for amelioration of obesity in mice. *Front. Microbiol.* **10**, 2155 (2019).
35. Donaldson, G. P. et al. Gut microbiota utilize immunoglobulin A for mucosal colonization. *Science* **360**, 795–800 (2018).
36. Peterson, D. A., McNulty, N. P., Guruge, J. L. & Gordon, J. I. IgA response to symbiotic bacteria as a mediator of gut homeostasis. *Cell host microbe* **2**, 328–339 (2007).
37. Peterson, D. A. et al. Characterizing the interactions between a naturally primed immunoglobulin A and its conserved Bacteroides thetaiotaomicron species-specific epitope in gnotobiotic mice. *J. Biol. Chem.* **290**, 12630–12649 (2015).
38. Ansaldo, E. et al. Akkermansia muciniphila induces intestinal adaptive immune responses during homeostasis. *Science* **364**, 1179–1184 (2019).
39. Lim, M. Y. et al. Gut microbiome structure and association with host factors in a Korean population. *Msystems* **6**, e00179–00121 (2021).
40. Callahan, B. J., McMurdie, P. J. & Holmes, S. P. Exact sequence variants should replace operational taxonomic units in marker-gene data analysis. *ISME J.* **11**, 2639–2643 (2017).
41. Kang, C.-s et al. Extracellular vesicles derived from gut microbiota, especially Akkermansia muciniphila, protect the progression of dextran sulfate sodium-induced colitis. *PloS one* **8**, e76520 (2013).
42. Watson, D. C. et al. Scalable isolation and purification of extracellular vesicles from Escherichia coli and other bacteria. *JoVE (Journal of Visualized Experiments)*, **176**, e63155 (2021).
43. Lane, R. E., Korbie, D., Trau, M. & Hill, M. M. Optimizing size exclusion chromatography for extracellular vesicle enrichment and proteomic analysis from clinically relevant samples. *Proteomics* **19**, 1800156 (2019).
44. Böing, A. N. et al. Single-step isolation of extracellular vesicles by size-exclusion chromatography. *J. Extracell. vesicles* **3**, 23430 (2014).
45. Gunther, P. et al. Structure of a bacterial Rhs effector exported by the type VI secretion system. *PLoS Pathog.* **18**, e1010182 (2022).
46. Koskiniemi, S. et al. Rhs proteins from diverse bacteria mediate intercellular competition. *Proc. Natl Acad. Sci.* **110**, 7032–7037 (2013).
47. Ma, J. et al. PAAR-Rhs proteins harbor various C-terminal toxins to diversify the antibacterial pathways of type VI secretion systems. *Environ. Microbiol* **19**, 345–360 (2017).
48. Yang, Y. et al. Focused specificity of intestinal TH17 cells towards commensal bacterial antigens. *Nature* **510**, 152–156 (2014).
49. Chung, H. et al. Gut immune maturation depends on colonization with a host-specific microbiota. *Cell* **149**, 1578–1593 (2012).
50. Xu, M. et al. c-MAF-dependent regulatory T cells mediate immunological tolerance to a gut pathobiont. *Nature* **554**, 373–377 (2018).
51. Miyoshi, Y. et al. Mechanisms underlying enhanced IgA production in Peyer's patch cells by membrane vesicles derived from Lactobacillus sakei. *Biosci., Biotechnol., Biochem.* **85**, 1536–1545 (2021).
52. Tan, J. et al. Dietary protein increases T-cell-independent sIgA production through changes in gut microbiota-derived extracellular vesicles. *Nat. Commun.* **13**, 4336 (2022).
53. Tett, A. et al. The Prevotella copri complex comprises four distinct clades underrepresented in westernized populations. *Cell host microbe* **26**, 666–679. e667 (2019).
54. Fehlner-Peach, H. et al. Distinct polysaccharide utilization profiles of human intestinal Prevotella copri isolates. *Cell host microbe* **26**, 680–690. e685 (2019).
55. Silby, M. W., Winstanley, C., Godfrey, S. A., Levy, S. B. & Jackson, R. W. Pseudomonas genomes: diverse and adaptable. *FEMS Microbiol. Rev.* **35**, 652–680 (2011).
56. Callahan, B. J. et al. High-throughput amplicon sequencing of the full-length 16S rRNA gene with single-nucleotide resolution. *Nucleic acids Res.* **47**, e103–e103 (2019).
57. Prodan, A. et al. Comparing bioinformatic pipelines for microbial 16S rRNA amplicon sequencing. *PLoS One* **15**, e0227434 (2020).
58. Nearing, J. T., Douglas, G. M., Comeau, A. M. & Langille, M. G. Denoising the Denoisers: an independent evaluation of microbiome sequence error-correction approaches. *PeerJ* **6**, e5364 (2018).
59. Toft, C. & Andersson, S. G. Evolutionary microbial genomics: insights into bacterial host adaptation. *Nat. Rev. Genet.* **11**, 465–475 (2010).
60. Kim, J.-S., Kang, S. W., Lee, J. H., Park, S.-H. & Lee, J.-S. The evolution and competitive strategies of Akkermansia muciniphila in gut. *Gut Microbes* **14**, 2025017 (2022).
61. Quast, C. et al. The SILVA ribosomal RNA gene database project: improved data processing and web-based tools. *Nucleic acids Res.* **41**, D590–D596 (2012).
62. Belforte, F. S. et al. Getting to know the gut microbial diversity of metropolitan Buenos Aires inhabitants. *Front. Microbiol.* **10**, 965 (2019).
63. Kenna, J. E. et al. Changes in the gut microbiome and predicted functional metabolic effects in an australian Parkinson's disease cohort. *Front. Neurosci.* **15**, 756951 (2021).
64. Pires, E. S. et al. The gut microbiome and metabolome of two riparian communities in the Amazon. *Front. Microbiol.* **10**, 2003 (2019).
65. Rubel, M. A. et al. Lifestyle and the presence of helminths is associated with gut microbiome composition in Cameroonians. *Genome Biol.* **21**, 1–32 (2020).
66. Turpin, W. et al. Associations of NOD2 polymorphisms with Erysipelotrichaceae in stool of in healthy first degree relatives of Crohn's disease subjects. *BMC Med. Genet.* **21**, 1–8 (2020).
67. Bian, G. et al. The gut microbiota of healthy aged Chinese is similar to that of the healthy young. *Msphere* **2**, 00327–00317 (2017).
68. de la Cuesta-Zuluaga, J. et al. Gut microbiota is associated with obesity and cardiometabolic disease in a population in the midst of Westernization. *Sci. Rep.* **8**, 11356 (2018).
69. Campbell, T. P. et al. The microbiome and resistome of chimpanzees, gorillas, and humans across host lifestyle and geography. *ISME J.* **14**, 1584–1599 (2020).
70. Bajer, L. et al. Distinct gut microbiota profiles in patients with primary sclerosing cholangitis and ulcerative colitis. *World J. Gastroenterol.* **23**, 4548 (2017).
71. Sepp, E. et al. Comparative analysis of gut microbiota in centenarians and young people: Impact of eating habits and childhood living environment. *Front. Cell. Infect. Microbiol.* **12**, 851404 (2022).
72. Saleem, A. et al. Unique Pakistani gut microbiota highlights population-specific microbiota signatures of type 2 diabetes mellitus. *Gut Microbes* **14**, 2142009 (2022).
73. Parker, E. P. et al. Changes in the intestinal microbiota following the administration of azithromycin in a randomised placebo-controlled trial among infants in south India. *Sci. Rep.* **7**, 9168 (2017).
74. Gaike, A. H. et al. The gut microbial diversity of newly diagnosed diabetics but not of prediabetics is significantly different from that of healthy nondiabetics. *Msystems* **5**, 00578–00519 (2020).
75. Galluzzo, P. et al. Comparison of the intestinal microbiome of Italian patients with multiple sclerosis and their household relatives. *Life* **11**, 620 (2021).
76. Quagliariello, A. et al. Gut microbiota composition in Himalayan and Andean populations and its relationship with diet, lifestyle and adaptation to the high-altitude environment. *J. Anthropological Sci.* **97**, 189–208 (2019).
77. Miyajima, Y. et al. Impact of gut microbiome on dyslipidemia in Japanese adults: Assessment of the Shika-machi super preventive

health examination results for causal inference. *Front. Cell. Infect. Microbiol.* **12**, 908997 (2022).
78. Dwiyanto, J. et al. Ethnicity influences the gut microbiota of individuals sharing a geographical location: a cross-sectional study from a middle-income country. *Sci. Rep.* **11**, 2618 (2021).
79. Jian, C. et al. Gut microbiota predicts body fat change following a low-energy diet: a PREVIEW intervention study. *Genome Med.* **14**, 54 (2022).
80. Doumatey, A. P. et al. Gut microbiome profiles are associated with type 2 diabetes in urban Africans. *Front. Cell. Infect. Microbiol.* **10**, 63 (2020).
81. Angelakis, E. et al. Gut microbiome and dietary patterns in different Saudi populations and monkeys. *Sci. Rep.* **6**, 32191 (2016).
82. Bressa, C. et al. Differences in gut microbiota profile between women with active lifestyle and sedentary women. *PloS one* **12**, e0171352 (2017).
83. Proffitt, C. et al. Genome-scale metabolic modelling of the human gut microbiome reveals changes in the glyoxylate and dicarboxylate metabolism in metabolic disorders. *Iscience* **25**, 104513 (2022).
84. Manor, O. et al. Health and disease markers correlate with gut microbiome composition across thousands of people. *Nat. Commun.* **11**, 5206 (2020).
85. Steele, M. I. & Moran, N. A. Evolution of interbacterial antagonism in bee gut microbiota reflects host and symbiont diversification. *Msystems* **6**, 00063–00021 (2021).
86. Cox, J. et al. Accurate proteome-wide label-free quantification by delayed normalization and maximal peptide ratio extraction, termed MaxLFQ. *Mol. Cell Proteom.* **13**, 2513–2526 (2014).
87. Proctor, A. et al. Resources to Facilitate Use of the Altered Schaedler Flora (ASF) Mouse Model to Study Microbiome Function. *mSystems* **7**, e0029322 (2022).
88. Tamura, K., Stecher, G. & Kumar, S. MEGA11: molecular evolutionary genetics analysis version 11. *Mol. Biol. Evol.* **38**, 3022–3027 (2021).
89. Letunic, I. & Bork, P. Interactive tree of life (iTOL) v3: an online tool for the display and annotation of phylogenetic and other trees. *Nucleic acids Res.* **44**, W242–W245 (2016).

Acknowledgements

This research was supported by the Main Research Program (Grant No. E0170600-08) of the Korea Food Research Institute funded by the Korean Ministry of Science and Information & Communication Technology (MSIT) (Y-DN), Bio & Medical Technology Development Program of the National Research Foundation (NRF) funded by the Korean Government (MSIT) (Grant No. NRF-2020M3A9G3080282) (K.S.K.), and Leaders in INdustry-university Cooperation (LINC) 3.0 project funded by the Ministry of Education (S.-N.L. & K.S.K.).

Author contributions

M.-G.H., E.-J.S. and H.J.Y. designed the study, performed the experiments, and analyzed the data. M-G.H., E-J.S., K.S.K., and Y.-D.N. wrote the manuscript. W.-H.C. contributed to experiments, data collection, and analysis. H.J.Y., H.Y.S., and K.S.K. managed the animal study and analyzed anti-commensal antibody response. H.Y.L. and S.I.K. assisted in proteomics data analysis. D.H.K. and D.K.L. contributed bacterial strains and performed EV production. G.J.K. and K.N.K. contributed T.E.M. analysis. J-G.S., S-N.L., K.S.K., and Y-D.N. oversaw all study design and data analysis. All authors have read and approved the final version of the manuscript.

Competing interests

M-G.H., D.H.K., D.K.L., S-N.L., and J-G.S. were employed by Enterobiome Inc. The authors declare that this study did not receive funding from Enterobiome Inc. The remaining authors declare no competing interests.

Additional information

Supplementary information The online version contains supplementary material available at https://doi.org/10.1038/s41467-025-57631-x.

Correspondence and requests for materials should be addressed to Sang-Nam Lee, Kwang Soon Kim or Young-Do Nam.

Peer review information *Nature Communications* thanks the anonymous reviewers for their contribution to the peer review of this work. A peer review file is available.